Applied Surface Science 360 (2016) 601–622

Contents lists available at ScienceDirect

Applied Surface Science

journal homepage: www.elsevier.com/locate/apsusc

A review on plasmonic metal–TiO_2 composite for generation, trapping, storing and dynamic vectorial transfer of photogenerated electrons across the Schottky junction in a photocatalytic system

L. Gomathi Devi *, R. Kavitha

Department of Post-Graduate Studies in Chemistry, Central College City Campus, Dr. Ambedkar Street, Bangalore University, Bangalore 560001, India

ARTICLE INFO

Article history:
Received 1 August 2015
Received in revised form 30 October 2015
Accepted 2 November 2015
Available online 10 November 2015

Keywords:
Metal deposition
Surface plasmon resonance
Schottky barrier
Vectorial charge transfer dynamics
Photocatalysis

ABSTRACT

The titania based nanomaterials are an attractive candidates for energy and environmental applications. TiO_2 is one of the most important photocatalyst for its special multiple characteristics like high reactivity, low toxicity, low cost, high flexibility, long term stability especially in aqueous medium, shows relatively high energy conversion efficiency, easy to prepare several modifications with various morphologies, with good recycle ability, favorable band edge positions and superior physicochemical and optoelectronic properties. However, large band gap of titania and massive charge carrier recombination impairs its wide photocatalytic applications. As an alternative to various strategies reported extensively in literature, noble metal deposition on the titania surface seems to be effective and reliable method for increasing the life time of excitonic pairs and to extend the band gap absorption to visible range of the solar spectrum. In this focused review, we discuss the fundamental and critical issues in the photocatalytic activity of metal deposited titania taking into consideration the influence of various parameters like preparation methods, metal dispersion on titania, formation of heterojunctions and optimum metal loadings on the interfacial charge carrier dynamics. The metal deposition onto the varied hierarchical morphology, crystal structure, defective surface of titania along with extended modification like simultaneous doping and heterostructure coupling with other semiconductors is also highlighted. It was revealed that deposited metal is involved in multiple crucial roles like; (i) it serves as passive electron sink with high capacity to store electrons to suppress photogenerated charge carrier recombination; (ii) it facilitates rapid dioxygen reduction to generate reactive free radicals; (iii) visible light response for titania can be achieved through surface plasmon resonance effect; (iv) direct excitation of metal nanoparticles especially under visible light and vectorial electron transfer to the TiO_2 CB. This review attempts to provide a comprehensive update of design and fabrication of metallization on the surface of TiO_2 semiconductor particles highlighting some of the advancements made in the energy and environment applications.

Contents

* Corresponding author.
E-mail address: gomatidevi_naik@yahoo.co.in (L. Gomathi Devi).

http://dx.doi.org/10.1016/j.apsusc.2015.11.016
0169-4332/

1. Introduction

Nano metal deposits on semiconductor surface provide a simple and convenient way to tailor the physicochemical-optical properties of the photocatalysts. A great deal of research on photocatalyst engineering has been carried out to customize the electronic band structure of various semiconducting materials for a specific chemical reaction with unique opto-electronic property [1,2]. TiO_2 is one of the most widely used semiconductor photocatalyst for the oxidative destruction and mineralization of vast number of organic substrates [3–8]. The main aim is to explore novel photocatalyst materials with suitable band structure which allows efficient photogeneration of electron–hole pairs to participate in oxidative/reductive processes preferably in the visible region [9–11]. The high charge-carrier recombination rate is the consequence of deeper penetration depth of photons (beyond the space charge region) and the short mean free paths of charge carriers, which stipulates the charge carriers to recombine before they could reach the semiconductor surface to participate in photochemical reactions [12]. Attempts to address this problem were mainly centered on fabricating the photocatalyst structure in order to maximize the photon absorption and minimize the charge carrier recombination. Apart from introducing various bulk imperfections via doping to provide shallow trap states for electrons, another effective method for increasing the life time of electron–hole pairs and to extend the band gap absorption of titania to the visible region is to deposit the noble metal on the titania surface [11–15]. Noble metals in bulk are photoactive only to a small extent but when deposited on the surface of semiconductors like TiO_2, possess electron storage properties leading to improved charge separation or charge rectification. The noble metal nanoparticles when deposited on the surface of the semiconductor have distinct optical and catalytic properties which are not usually observed in the case of bulk metal. Gerisher has highlighted the importance of dioxygen reduction by conduction band (CB) electrons which prevent the recombination of photogenerated charge carriers and he further inferred that the superoxide radical formation may be the slowest step in the reaction sequence occurring in the millisecond time regime leading to the oxidation of substrates [16]. A nano noble metal deposit on TiO_2 surface can enhance the photocatalytic efficiencies due to the faster rate of interfacial electron transfer from semiconductor to metal deposits and vice versa compared to the surface trapping states induced by the bulk modification [16]. The metal nano particles deposited on the TiO_2 surface change the original charge carrier concentration equilibrium by withdrawing the electrons out of TiO_2 bulk structure which in turn accelerate the dioxygen reduction. In any photocatalytic process involving metal/TiO_2 composite, deposited noble metal has the mediating role in trapping and transfer of photogenerated electrons from the TiO_2 to an acceptor. These activities greatly reduce the possibility of electron–hole recombination resulting in efficient separation and enhancing the rate of photocatalytic reactions [17]. In general, metallization decreases the probability of charge carrier recombination and increases the fraction of photogenerated holes undergoing the interfacial charge transfer reaction resulting in faster degradation of organic intermediates. Metal deposition on TiO_2 surface does not significantly alter the structure and microstructure of TiO_2, although marginal changes in surface area and pore diameter can be observed in most of the cases which are not large enough to influence the photoactivity in a drastic way [18]. Hence, it can be tentatively proposed that the deposited metals exert a more significant effect in the separation of photogenerated charge carriers and also on the catalysis process. The absorption properties of metallized TiO_2 depend on the optical properties of the deposited metal, the matrix and the volume fraction of the metal in the composite mixture. Metal deposited TiO_2 shows an absorption band in the visible region due to surface plasmon resonance (SPR) effect [19]. SPR is a characteristic feature of any metal nanoparticle deposited on semiconductor and this effect arises as a result of collective modes of oscillation of the free CB electrons induced by its interaction with electromagnetic field [20]. At the semiconductor/metal interface a significant redistribution of charge occurs due to the overlap of the wave functions from the two sides, depending on the work function of metal and semiconductor. The formation of a depletion zone causes the bending of valence band (VB) and CB of semiconductor for example in an n-type semiconductor the bands are shifted downwards and p-type semiconductors the bands are bent upwards in relation to the Fermi level [20]. The transfer of the photoexcited electrons from the CB edge of the semiconductor to the metal deposit is facilitated when the band edge positions of both match with each other, but the opposite scenario is prevented to certain extent by the formation of Schottky barrier [21]. The interaction of the CB electrons with the electromagnetic field of specific wavelengths in the nano metal deposits causes coherent electron cloud oscillations leading to the increase in the energy density at the surface. Thus, noble metal nanoparticles immobilized on the semiconductor surface can enhance the local field energy under visible light excitation through the SPR effect and then these electrons participate in the photocatalytic redox reactions or in the energy conversion process [22]. The plasmon absorption band of metal deposited TiO_2 will be generally observed at higher wavelengths compared to the unmodified TiO_2. Interfacial and interparticle interactions dictate the shift and broadening of plasmon band of metal nanoparticles deposited on the TiO_2 surface [23]. The choice of noble metal for the surface deposition to enhance the photocatalytic activity of TiO_2 depends on its work functions, size and shape which in turn influences the optical properties of TiO_2 [24,25]. Highly dispersed metal nanoparticle on the semiconductor surface will have low degree of aggregation due to the stabilization provided by the surface charges and further it prevents the scattering effects and allows the efficient absorption of photons by the metal/TiO_2 composite system. The chemical transformations of the substrate molecules at the metal/TiO_2 interface may be detrimental to the long-term stability of the metal/TiO_2 heterojunction, since the transformations may alter the valency of the metal species during the photocatalytic reactions [26]. Since the experimental conditions like reaction medium, redox species at the interface and the intensity of excitation directly influence such chemical transformations, it is necessary to consider these issues while designing a composite photocatalyst for long term irradiation experiments. Photometallization process carried out for longer duration (under UV irradiation) results in a decrease in the efficiency of photoelectrochemical and photocatalytic activity. The possibilities of oxidation of deposited metal by the photogenerated hole and/or surface hydroxyl radicals was proposed as the reason for the observed deterioration of the catalytic performance of the nanocomposite [27]. In this regard researchers have used several noble metals like Pt, Au, Pd and Ag for deposition on TiO_2 surface. The advantages and limitations of each metal deposited on TiO_2 surface is discussed elaborately in further sections.

2. Photocatalytic activity of platinum deposited titania (Pt/TiO_2)

It is well known that Pt is one of the best noble metal catalyst used in the conventional thermal oxidation processes. Deposition of Pt on TiO_2 surface is thought to enhance charge carrier separation and increase the extent of surface adsorption of various organic compounds. Pt serves as an electron trap forming a charge-transfer complex between Pt and TiO_2 [27–31].

Sakata et al. discussed the photocatalytic properties of Pt loaded TiO_2 particles in terms of photochemical diode [27].

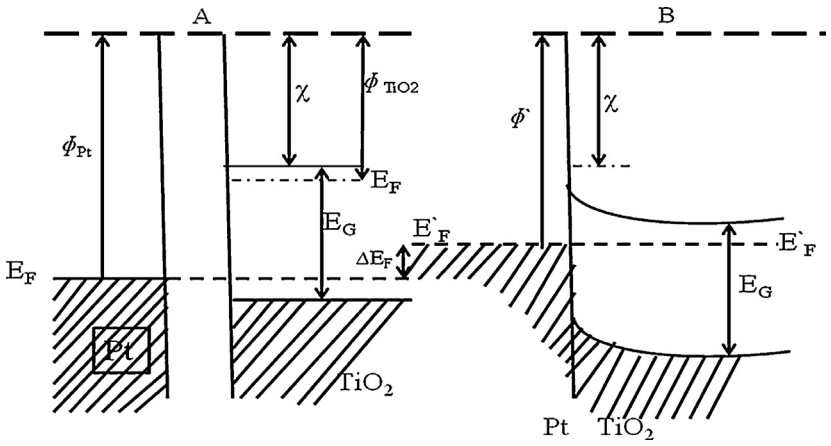

Fig. 1. Energy band diagram under UV illumination: (A) before contact between Pt and TiO_2, (B) after contact between Pt and TiO_2. χ and E_G are the electron affinity and energy band gap of TiO_2, respectively. Φ_{TiO2} is the work function of illuminated TiO_2. Φ_{Pt} is the work function of Pt. $\Delta E_F = \Phi_{Pt} - \Phi_{Pt}$, is the increase in the Fermi level of Pt after contact with illuminated TiO_2.

Reprinted with permission from Ref. [28] Copyright (1983) Royal Society of Chemistry.

This model describes the formation of Schottky barrier at the metal–semiconductor interface with the creation of an electron depletion layer at the Pt/TiO_2 junction leading to the downward bending of TiO_2 energy bands (Fig. 1) [28]. Electrons are readily transferred through this heterojunction barrier and are trapped by the Pt nanoparticles, while the photogenerated holes are directed toward the interface. Thus, metal deposits serve as passive electron sinks and enhance the kinetics of dioxygen reduction (cathodic half reaction in the photocatalytic process), while the holes tend to accumulate at the TiO_2-solution interface [28].

$$ne^- + M^0 \rightarrow M^{n-} \quad (1)$$

$$M^{n-} + O_2 \rightarrow {O_2}^{-\bullet} + M^0 \quad (2)$$

The dioxygen reduction by photoelectrons can induce multistep chain reactions producing various kinds of oxidative free radicals, which reinforces the process of anodic oxidative photodecomposition of the substrate molecule [27]. Thus based on the photochemical diode model, anodic oxidation and cathodic reduction takes place at the metal and TiO_2 surface, respectively under UV light illumination. At the interface of two materials, electrons flow from one material to another (from the higher energy Fermi level to lower energy Fermi level) to equilibrate the Fermi energy levels. Charge accumulation on the metal results in the Fermi-level equilibration by raising the quasi Fermi level of the metal close to the CB energy level of the oxide semiconductor [29]. The charges at the Helmholtz and diffuse double layers formed at the metal-solution interface play an important role in controlling the Fermi-level equilibration [30]. Schottky barrier formed at the heterojunction results in the metal having an excess negative charge and the semiconductor with an excess positive charge, between which a depletion layer is formed that maintains the charge separation. The negative charge on the metal nanoparticles is also due to the large difference in the work function of deposited metal and the TiO_2. Thus, electron transfer is facilitated from the material with higher work function to the material with lower work function [31]. Pichat et al. analogously observed a decrease in the photoconductivity of platinized TiO_2 samples in comparison with pure TiO_2 due to the flow of electrons from TiO_2 to metal [28]. Literature also shows the reduction of water to oxygen with irradiated Pt-loaded rutile TiO_2 [32–35]. In these experiments the flat band potential of TiO_2 single crystal having rutile structure was observed at a potential slightly positive with respect to the Hf^+/H_2 redox potential [32]. Pt deposition carried out by Ohtani et al., on different crystal phases of titania (either on the surface of anatase or on the surface of rutile) did not influence the electron transfer process from TiO_2 to Pt [33]. This conclusion was based on the results obtained for both these samples which showed similar activity for H_2 evolution based on the action spectral studies [33]. Moonrisi et al. reported the enhanced rate of degradation of 4-chlorophenol (4-CP) using Pt deposited (1 mol%) P 25 under the experimental conditions of nitrogen bubbling. They observed that the degradation rate decreased in the presence of dissolved oxygen [34]. In another study Pt/TiO_2 (rutile) showed superior activity for CO conversion, while only 75% of CO conversion was achieved with Pt/P25. But however Pt/TiO_2 (anatase) showed no activity at all under visible light irradiation. In this case, Pt/TiO_2 (rutile) can be considered as a multifunctional catalyst, since rutile phase can be activated by the visible light and the deposited Pt facilitates both CO adsorption and charge transfer process [35]. Bosc et al. also reported similar results with Pt/P25, which showed lower activity compared to Pt/TiO_2 (rutile) photocatalyst for CO conversion, probably due to the poor absorption of the former under the stream of visible light illumination [36]. It is suggested that Pt deposits on the surface of anatase crystals of P25 may not maintain its metallic state and they do not have physical metal semiconductor interface compared with the visible light photoactivated rutile. Anatase phase is not photoactive under visible light illumination and further the Pt metal deposits are oxidized on the surface as PtO_x species resulting in lower CO uptake [35]. Pt deposited (1 wt%) Hombikat UV 100 (pure anatase) and Millenium PC 50 (pure anatase) showed enhancement for the decomposition of phenol and total organic carbon removal by a maximum factor of 1.5 compared to the unmodified titania [37]. While Pt deposited P25 sample containing both anatase and rutile phases showed lower activity compared to the undeposited P25, which suggested that platinization did not increase the efficiency of charge separation in Pt/P25 and the bicrystalline framework itself was sufficient enough to hinder the efficient charge recombination in photocatalytic reaction [37]. Sakthivel et al., has demonstrated that Pt loading on P25 (0.8 wt%) increases the activity of the catalyst for the photodegradation of Acid Green 16 [38]. Li and Li have found that Pt (0.75%) deposited on biphasic TiO_2 (85% A + 15% R) showed superior activity for the degradation of methyl orange (MO) and methylene blue (MB) under UV/visible light irradiation [39]. From the XPS studies it is shown that the partial reduction of $PtCl_6^{2-}$ takes place during the photodeposition process and results in the formation of $Pt(OH)_2$, PtO_2 along with metallic Pt on TiO_2 surface and also leads to the formation of Ti^{3+} centers in the crystal

lattice [40]. According to them, these impurities served as visible light harvesters and also effectively inhibited the charge carrier recombination resulting in the enhanced activity compared to bare TiO_2. Based on cryo-TEM studies, Wang et al., suggested that TiO_2 nanoparticles tend to form three dimensional networks in the solution which is considered as antenna system leading to the improved photocatalytic activity [41]. The deposition of Pt apparently favors the particle aggregation to form the chain structures which are pre requisite for the fast transport of excitation energy or photogenerated charge carriers. Choi and co-workers reported that Pt metallization effect is nearly nil and it is even negative with rutile TiO_2, while the effect was consistently positive with anatase TiO_2 for the dechlorination of trichloroethylene (TCE) irrespective of the light intensity [42]. The degradation of TCE on the surface of platinized TiO_2 showed positive results at high light intensity, but showed poor activity at low light intensity. In another study polyoxometallate (POM) is used as an electron shuttle mediator for the photocurrent in Pt/TiO_2 suspension. When the TiO_2 surface is platinized, the photocurrent is expected to increase because of the CB electron trapping by the Pt deposits [43]. As the number of CB electrons increases they are transferred to the collector electrode via redox cycle of POM or to the Fe^{3+} ions. Fe^{3+} ions mediated photocurrent generation in the Pt/TiO_2 suspension was consistently more efficient than that of TiO_2 suspension under all irradiated conditions and this is due to the scavenging ability of Fe^{3+} ions for the CB electrons. Photocurrent generation with Pt/TiO_2 system is higher for low intensity light compared to high intensity light suggesting significant enhancement in photocurrent generation when the photon flux is limited [44]. Pt/TiO_2 facilitated the reaction process for trapping of CB electron by TCE molecule to generate TCE radical. Further, when TCE radical reacts with VB hole (TCE mediated recombination) on the surface, results in a null reaction and the overall efficiency of TCE degradation is reduced. Once TCE radical is desorbed from the Pt surface into the bulk liquid, it immediately reacts with oxygen and will have very little chance to readsorb on TiO_2 surface. Therefore, oxidation of TCE radical either takes place on the Pt surface leading to the null reaction or in the bulk of the reaction solution leading to complete oxidation. The null reaction pathway occurring on Pt/TiO_2 surface is favored under low intensity light. The trapping of more number of electrons by Pt deposit by using high intensity light induces negative charge on the TiO_2 surface and hence destabilizes TCE radical anion due to electrostatic repulsion [45]. Photoplatinization of TiO_2 thin films using water/ethanol (acts as sacrificial electron donor) solutions in the molar ratio of 80/20 showed superior biregime activity for Orange G degradation under UV irradiation [46]. Pt/TiO_2 thin film prepared by using pure ethanolic solution and 50% ethanolic solution showed lower activity suggesting that platinization in water rich environment is more favored [47]. However, such biregime photocatalytic mechanism was not observed for non-platinized TiO_2 thin films due to the poor rate of photoelectron transfer to dissolved oxygen. Photoplatinization in ethanol rich solution induced CO adsorption (by product of ethanol oxidation) at the surfaces of Pt clusters and total desorption of CO requires high thermal treatment. Conversely, photo platinization in water rich environment suppress the CO contamination and seems to promote water adsorption at the surface of Pt clusters which favors hydroxyl radical generation. CO adsorption in the former case hampers the process of photoelectron transfer to the dissolved oxygen thereby reducing the efficiency [47]. Superior activity was observed when deposit size was 2.5–4 nm for the degradation of phenol compared to the samples with higher deposited sizes (4–8 nm) obtained at higher calcination temperature [48]. This could suggest that within the same sample there is an optimum size for metal deposits for improved photoefficiency and the larger metal deposits might become detrimental [49]. The Pt deposition before sulfation on TiO_2 surface showed higher photoactivity for acetone oxidation compared Pt deposition after sulfation. In this case Pt was deposited on the TiO_2 surface via $NaBH_4$ reduction [50]. In the former case, boron species were removed during sulfation process, while in the later case, boron species served as recombination centers during the process of oxidation of acetone. The degradation of trichloroacetate (TCA) under UV illumination revealed that anoxic path was dominant on platinized TiO_2, while the oxic path was operative on bare TiO_2. It was suggested that platinum surface stabilized reactive intermediates (dichlorocarbene) and subsequently changed the mechanistic pathway of TCA degradation. However, the presence of electron donors favored oxic pathway for both the photocatalysts, as they scavenged the VB holes [51]. Linsebigler et al., showed that the addition of Pt particles to TiO_2 single crystal surface decreased both the rate and total yield of the photooxidation of CO [52]. It was proposed that the defect sites (Ti^{3+}) which are necessary for the oxidation of CO to CO_2 was preferentially blocked by Pt particles which reduces the photoreactivity of the catalyst. Pt deposited TiO_2

Table 1
Characteristics of bare and Pt/TiO_2 samples before and after the photocatalytic oxidation of DMMP.

Photocatalyst	S_{BET}, m^2/g	Pt oxidation state	Pt oxidation state[a]	[Pt]/[Ti]	[Pt]/[Ti][a]	W_{max}, mol/cm^2 s $\times 10^{10}$	$n(CO_2)$, mol/cm^2 $\times 10^7$
P25	57	–	–	–	–	1.6	1.1
SCR	57	Pt^0, Pt^{1+}	Pt^0, Pt^{1+}	0.013	0.012	3.1	4.3
PD	57	Pt^{2+}	Pt^0, Pt^{2+}	0.010	0.003	2.4	2.5

Reprinted with permission from Ref. [55] Copyright (2011) Elsevier.
W_{max} is the maximum rate of the CO_2 production registered during photocatalytic oxidation.
[Pt]/[Ti] are the atomic ratios of the respective cations on the surface of Pt/TiO_2 according to XPS measurements.
$n(CO_2)$, mol/cm^2 $\times 10^7$ is the amount of CO_2 evolved in 1600 min.
[a] The oxidation state after the reaction.

Table 2
Physico-chemical properties and photocatalytic activities of fibrous TiO_2 and Pt/TiO_2 prepared by using $H_{2-2x}[Pt(NH_3)_4]_xTi_4O_9 0.25H_2O$ precursor.

Preparation conditions	Phase compositions[a]	SSA, m^2/g	Band gap (eV)	H_2 evolution ability (mmol h^{-1})	NO destruction ability (%)	
					>400 nm	>290 nm
P25	A + (R)	47.3	3.04	0.032	37.0	51.2
Fibrous TiO_2 treated in methanol at 325 °C	M + (A)	22.1	3.31	0.311	5.2	30.1
Fibrous TiO_2/Pt treated in methanol at 325 °C	A + (M + H8 + R)	24.0	3.31	2.540	9.0	46.0

Reprinted with permission from Ref. [62] Copyright (2005) Elsevier.
The phase described first is the major product and that in parenthesis is the minor product.
[a] A: anatase TiO_2; M: monoclinic TiO_2; R: rutile TiO_2; H8: $H_2Ti_8O_{17}$.

is also reported to be less effective in the photooxidation of gas-phase TCE under broad-band irradiation ($\lambda > 300$ nm) compared to TiO_2 [53]. The ratio of $CO_2/COCl_2$ increased as a function of Pt loadings, suggesting that extent of Pt loading affects the distribution of photoproducts. The change observed in the product distribution in this case could be due to the extent of $COCl_2$ adsorption on the surface of Pt particles [54]. To study the difference in the chemical state of Pt and the dispersion pattern, the method of platinization (2 wt%) was carried out by both soft chemical reduction method (SCR) and also from photodeposition (PD) method (Table 1) [55]. It was observed that both Pt/TiO_2 samples showed enhanced photooxidation of dimethyl methyl phosphonate (DMMP) under UV light irradiation. However, XPS studies revealed that SCR method leads to the deposition of metallic Pt whereas PD method results in the deposition of Pt as Pt^{2+}. In the course of the photocatalytic oxidation of DMMP the metallic state of Pt (SCR) remains stable and unchanged for long time. On the contrary the photocatalyst prepared via PD method is deactivated quite rapidly due to the reduction of Pt^{2+} to Pt^0 which led to the agglomeration of Pt nanoparticles [55]. Pt (1 at%, 5 nm size)/TiO_2 nanowire hybrids fabricated by chemical reduction method showed enhanced photocatalytic degradation of MB under UV light [56]. Photogenerated electrons are transported at a faster rate through Schottky barrier to Pt deposits and in turn they are transferred to dissolved oxygen molecules [57]. When the Pt loading was above 1 at%, the deposit would simultaneously attract both electrons and holes and acts as recombination center in spite of enhanced response to the visible light [58]. The FTIR spectra of Pt/TiO_2 and TiO_2 samples (taken after the process of photodegradation) suggested that $-CH_3$ group of MB is adsorbed on the surface and it can be oxidized completely to CO_2 more efficiently by Pt/TiO_2 rather than TiO_2 due to the superior catalytic activity of Pt [56]. Pereira et al., have shown that Pt/TiO_2 nanoparticles prepared by the polymer precursor method demonstrated efficient photocatalytic degradation of MO under UV light irradiation compared to TiO_2 [59]. The PXRD patterns indicated the incorporation of Pt into the TiO_2 lattice along with a small amount of rutile phase formation when the concentration of Pt was less than 1 mol% and metallic Pt deposition takes place when the concentration was higher than 1 mol%. When the concentration of Pt exceeds the optimum limit, phase segregation occurs on the surface of TiO_2 since the Pt clusters are expelled due to its high density from the TiO_2 bulk lattice. The high photocatalytic activity of these Pt/TiO_2 photocatalysts were attributed to the electronic defects created by the doping mechanism at low Pt content and due to the effective charge transfer mechanism at the metal/oxide interface at high Pt concentration level [60]. Their work showed that both doped and metalized samples had similar photocatalytic activity [59]. Self decorated Pt (0.2 at%) metal deposits on the surface of TiO_2 prepared by anodization of Ti–Pt alloy for 2 h exhibited enhanced photocatalytic hydrogen evolution under both UV/visible light irradiation [61]. These Pt nanoparticle deposits were found to have a diameter of 4–5 nm with inter particle spacing of ~50 nm and these dimensions were partially adjustable by changing anodization conditions. Samples prepared at shorter (~30 min) and longer (~4 h) anodization time periods exhibited lower hydrogen production which indicates the need of optimum size with particle interspacing for effective photocatalytic performance [61]. Fibrous titania loaded with 1 wt% Pt prepared by the solvothermal reaction using two different precursors independently like either $H_{2-2x}[Pt(NH_3)_4]_xTi_4O_9 0.25H_2O$ or $H_2Ti_4O_9 0.25H_2O$/Pt in methanol medium at 350 °C exhibited higher hydrogen evolution rates when compared to the samples prepared either by calcination or by hydrothermal treatment [62]. However the photocatalytic activity of Pt/TiO_2 prepared by using the precursor $H_{2-2x}[Pt(NH_3)_4]_xTi_4O_9 \cdot 0.25H_2O$ was higher than that of $H_2Ti_4O_9 0.25H_2O$/Pt as precursor due to the difference in the valence state of Pt. These catalysts when used for NO destruction showed modest activity due to low specific surface area. The sample prepared by using $H_{2-2x}[Pt(NH_3)_4]_xTi_4O_9 \cdot 0.25H_2O$ precursor in methanol at 350 °C contains a mixture of monoclinic titania, protonic octatitanate, anatase and rutile phases, suggesting that the phase transformation of tetratitanate was accelerated by the existence of Pt (Table 2). In addition to phase transformation process, the reduction of Pt ion to metallic Pt could also proceed simultaneously resulting in uniform distribution of Pt fine particles on the surface of titania particles [62]. Pt/TiO_2 films supported on hydroxylated fly ash cenospheres (FACs) (alumina silicate rich byproducts generated in coal firing poder plants) exhibited enhanced photodegradation of MB under visible light irradiation [63]. The deposition of Pt^0 effectively narrowed the band gap by promoting the formation of Ti^{3+}. The photodegradation rate of MB increased with pH in aqueous solution which was attributed to the improved ability of Pt/TiO_2 to adsorb MB at alkaline pH [64]. The effects of various inorganic anions on the photodegradation reaction were studied and the rate shows the following order: $HCO_3^- > F^- > SO_4^{2-} > NO_3^- > Cl^-$. Photocatalytic degradation rate decreases at higher anion concentration due to the ability of anions to scavenge the hydroxyl radicals and holes. The Pt/TiO_2 supported on hydroxylated low density FACs floats on the surface of water favoring higher extent of absorption of sunlight in the practical applications [65].

Justin and co-workers interpreted charge carrier separation mechanism in terms of charge carrier decay for short and long time duration based on time resolved microwave conductivity studies [66]. In the short time range (1–40 ns) few electrons can be trapped by the activated metal and few charge carriers are lost in the faster recombination. In long time range (40–100,000 ns), the process of decay takes place between trapped species and the decay of the excess electrons is controlled by their slow recombination with either trapped or relaxed holes. The predominant negative effect in the short time range seems to be produced by the rutile phase and also platinization in the case of P25. In the long-time range, platinization had different effects on different catalysts. Separation of charge carriers was efficient in PC50, it was insignificant in the case of P25 and decay of electrons was accelerated in the case of UV 100. The observed activity is the resultant effect of both the negative and positive effects of platinization [66]. However, contrast to these reports, Chen et al. observed an increased rate of photocatalytic oxidation of methanol and ethanol on platinized P25, but the same catalyst was less effective for the degradation of chloroform compared to bare P25 [67]. Mesostructured Pt (0.5 wt%)/TiO_2 nanocomposites with anatase/rutile ratio of 65.5/34.5 (from XRD data) prepared by simple one step sol–gel reaction (annealed at 450 °C in the presence of H_2 gas for 2 h) yielded highly crystalline ordered hexagonal mesoporous TiO_2 (confirmed by TEM) [68a]. The photocatalytic activity was evaluated by measuring the initial rate of HCHO formation generated by photooxidation of CH_3OH in aqueous suspension. The photocatalytic activity of 0.5 wt% Pt deposited TiO_2 nanocomposites were found to show significantly higher activity (three times) than that of 0.5 wt% Pt deposited colloidal UV-100 Hombikat or Aeroxide TiO_2 P25. This superiority was attributed to the anatase–rutile bicrystalline framework, large surface area, high crystallinity and mesoporous structure [69]. It was observed that in this three-dimensional solid/surface state framework, the excited TiO_2 nanoparticle can transfer the absorbed energy through the mesoporous hexagonal TiO_2 network to the other TiO_2 in the ground state. This antenna mechanism results in energetic coupling which extends throughout the three-dimensional TiO_2 network. This will enable the energy and/or exciton transfer from the particle where the initial photon absorption took place to the particle where the electron transfer process finally occurs. Further, the probability of electron transfer to the Pt particle is increased by an increased CH_3OH diffusion through

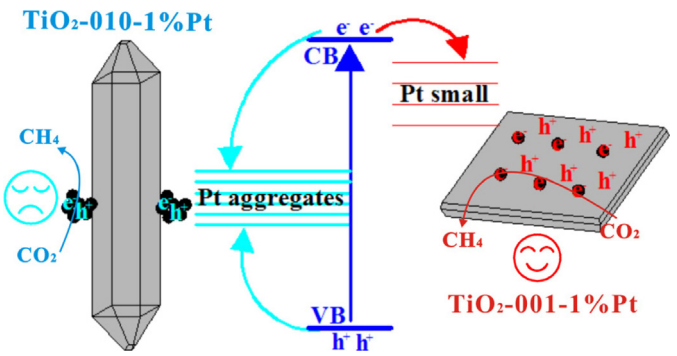

Fig. 2. Mechanism for the reversed photoactivity order of anatase TiO_2 {0 0 1} and {0 1 0} facets on Pt/TiO_2 during the photocatalytic CO_2 reduction process.
Reprinted with permission from Ref. [73] Copyright (2014) Elsevier.

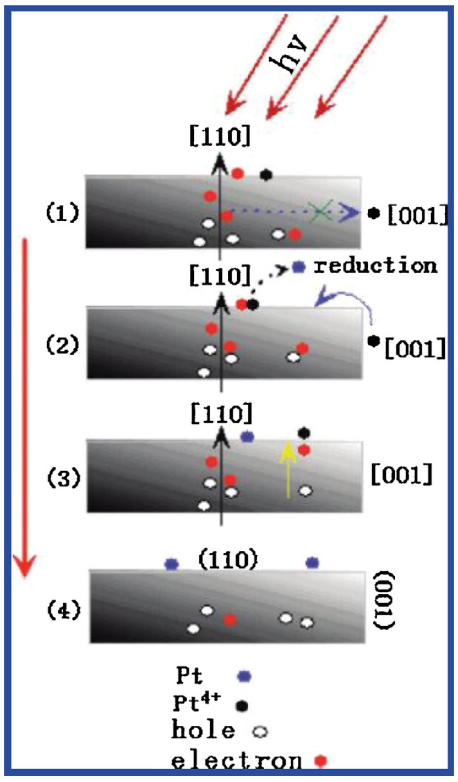

Fig. 3. Scheme of photoreduction process designed for Pt deposition onto the microspheres of TiO_2.
Reprinted with permission from Ref. [76] Copyright (2011) American Chemical Society.

the pores of the nanostructures. Once the electron has reached the Pt particle in the presence of adsorbed methanol, which is known to act as hole trap induces the charge separation of the original exciton. The overlap of the energy bands of the TiO_2 nanoparticles forming the three dimensional network will result in unified energy bands for the entire system enabling a quasi-free movement of the photogenerated charge carriers throughout the system [70]. Hierarchically macro-/mesoporous Pt/TiO_2 showed enhanced thermal catalytic activity toward the catalytic decomposition of HCHO compared to DP25 mainly attributed to the hierarchically arranged macro-/mesoporous structures on the TiO_2 support, large specific surface area and optimal pore size [68b]. Yu et al., reported the use of Pt/TiO_2 nanosheets with exposed {0 0 1} facets for H_2 production in the presence of sacrificial agents (electron acceptors) like glycerol, triethanolamine and glucose [71]. The photodeposition of Pt on TiO_2 although found to enhance the photocatalytic activity, it is still controversial as to whether Pt/TiO_2 interface forms an ohmic contact or Schottky barrier [72]. Mao et al., reported that Pt-loaded anatase TiO_2 with (0 0 1) and (0 1 0) facets showed reverse photocatalytic activity for photoreduction of CO_2 to CH_4 [73]. It was observed that TiO_2 (0 1 0) facet without Pt-loading exhibited higher photocatalytic CO_2 reduction efficiency which was attributed to its larger CO_2 adsorption capability and longer photogenerated charge carrier lifetime when compared with TiO_2 (0 0 1) [74]. Whereas the photoinduced charge carrier separation was more efficient with platinized TiO_2 (0 0 1) facet when compared to the activity of platinized TiO_2 (0 1 0) facet. The above results provide an important indication about the effects of Pt-loading on the anatase TiO_2 for the photocatalytic CO_2 reduction with different exposed facets. The results also shed light on the fabrication of novel nanostructured photocatalysts through crystallographic morphology control for high conversion efficiency in the CO_2 resource utilization. The TiO_2 (0 0 1) facets shows uniform and regular Pt nanoparticles on its surface, while the TiO_2 (0 1 0) facets had agglomerated Pt nanoparticles (for 1 wt% Pt deposition) and this difference was due to their different surface electronic structures (Fig. 2) [75]. A well distributed smaller Pt nanoparticles on TiO_2 (0 0 1) facets was an important factor to enhance the lifetime of charge carrier as compared to the agglomerated Pt nanoparticles loaded on TiO_2 (0 1 0) facets [73]. Zhang et al., reported a two stage strategy toward the selective Pt deposition on the assembled microspheres of TiO_2 (1 1 0) facet which exhibited an excellent photocatalytic activity for MO degradation under UV/visible light irradiation [76]. This approach included the assembly of nanowires with exposed (1 1 0) facet and (0 0 1) tips to form microspheres followed by Pt deposition only on the (1 1 0) facet by the photoreduction method. The rutile TiO_2 microspheres constituting nanowires with special structure provides two possible directions along (1 1 0) and (0 0 1) for the migration of the electrons. Initially (1 1 0) facet will be enriched by electrons, since it is an efficient reduction facet for rutile TiO_2 as indicated by the reduction of Fe^{3+} to Fe^{2+} in the photoreaction process. Thus, it was believed that photogenerated electrons could predominantly be

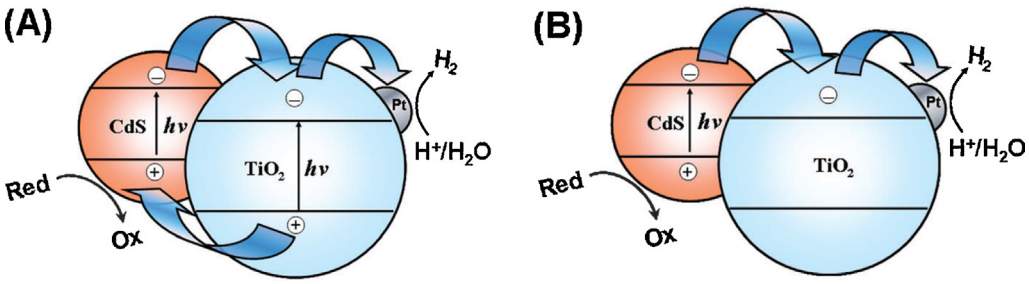

Fig. 4. Interfacial charge transfer mechanism in CdS/Pt/F^-/TiO_2 under UV (A) and visible-light (B) irradiation.
Reprinted with permission from Ref. [79] Copyright (2014) Wiley Publications.

spread along the (1 1 0) direction rather than (0 0 1) direction. This is because the (1 1 0) surface of each nanowire possess high energy to spread the electrons from nucleation center to microsphere surfaces (Fig. 3). Further, it is well-known that Ti atoms show 6-fold coordination and oxygen atoms are 3-fold coordination in rutile TiO_2. The nanowires terminating at (1 1 0) may break the Ti—O bonds which lie normal to the surface plane and results in 5-fold coordination for Ti and 2-fold coordination for O atoms on the surfaces [77]. The lower coordinated bridging oxygen atoms at surface of (1 1 0) facet may form a minimum energy position for a single Pt atom. Therefore, at terminal plane, microspheres were assembled by bundles of nanowires with special growth direction which could be suitable for Pt deposition. Upon Pt deposition, the dielectric permittivity was further improved and the work function for Pt metal is 5.36 eV which is higher than the work function of (1 1 0) surface facet (4.2 eV) of rutile TiO_2 [78]. The position of CB energy of TiO_2 microspheres is located above the Fermi level of the Pt nanoparticles and the Pt deposition leads to the formation of a Schottky barrier at metal/semiconductor contact leading to the transfer of electrons from TiO_2 CB to Pt nanoparticles, while the reversible process can be extremely difficult unless the band energy positions are equalized. A Pt nanoparticle initially gets excited under visible-light irradiation because of the SPR effect. Then excited electrons may transfer from the lower energy bands of Pt (below the Fermi level) to its higher energy level. These activated electrons at higher energy levels get migrated from Pt deposits to the CB of TiO_2 microspheres. Subsequently, these electrons could be directly captured by adsorbed O_2 molecules at the vicinity of microsphere surfaces to form the superoxide radical species for the photocatalytic reactions. The time taken for producing the photoexcited electrons is much shorter in comparison to the reaction time to generate the superoxide radical species and to decompose the MO molecules. Therefore, accumulation of extra electrons is highly possible situation for compensating the time difference. In this regard, the microcapacitors are formed in the adjacent nanowires within microspheres and the enhanced dielectric constant upon Pt deposition could provide a huge electronic storage. In this case of visible-light irradiation, owing to the continuous electronic migration from Pt nanoparticles to TiO_2 CB, Pt nanoparticles may exert some degree of positive charges. The electronic donors like H_2O or HO^- in the MO solution would readily provide electrons to Pt metal to form the hydroxyl radicals, since the potential of the above donors is more negative than that of the holes in the Pt nanoparticles. These highly activated radicals could participate in the photocatalytic reaction for effective removal of MO species [75]. CdS-sensitized $Pt/F^-/TiO_2$ nanosheets with exposed (0 0 1) facets is fabricated by a three-step procedure: TiO_2 nanosheets were prepared from $Ti(OC_4H_9)_4$, HF and H_2O reactants and the mixture is subjected to hydrothermal treatment followed by Pt metallization by photochemical reduction method and the deposition of CdS nanoparticles is done by the chemical bath method [79]. $CdS/Pt/F^-/TiO_2$ nanosheets exhibited enhanced photocatalytic hydrogen evolution rate under UV/visible light irradiation and this enhancement is attributed to: (i) the presence of exposed (0 0 1) facet, (ii) surface fluorination and (iii) high specific surface area. Further the beneficial effects of Pt deposition are: (i) improved the charge carrier separation, (ii) reduced the hydrogen production over potential and (iii) suppresses the reverse reaction of O_2 and H_2. Under UV irradiation, both TiO_2 nanosheets and the deposited CdS nanoparticles undergo photoexcitation simultaneously producing electrons and holes in their corresponding CB and VB, respectively (Fig. 4). Due to the difference in band edge positions the excited electrons gets transferred from the CB of CdS to the CB of TiO_2. Contrarily, the created holes from the VB of TiO_2 migrate to VB of CdS. Finally all these excited electrons migrate to the deposited Pt nanoparticles to react with the adsorbed H^+ ions to form H_2. The Pt on TiO_2 nanosheets induces a Schottky barrier, which facilitates electron capture while the accumulated holes in the CdS VB leads to the oxidative decomposition of lactic acid or any other pollutant [80,81]. However, under visible light irradiation only CdS nanoparticles with low band gap gets photoexcited to produce electrons in CB and holes in the VB, respectively. These electrons in the CdS CB transfer to TiO_2 CB and then migrate to Pt nanoparticles to reduce H^+ to yield H_2. The photocatalytic activity of $CdS/Pt/F^-/TiO_2$ in the presence of model electron donors or scavengers like triethanolamine, glucose, glycerol and mixed Na_2S–Na_2SO_3–H_2O solutions exhibited the hydrogen production rates of 75.6, 38.6, 11.8, and 25.8 mmol h^{-1}, respectively. However the hydrogen production rate in the presence of lactic acid is found to be 265 mmol h^{-1} which is very much higher than the above mentioned electron scavengers. In addition to hydrogen evolution process, simultaneous decomposition of pollutants can also be accomplished. The F^- ions adsorbed on TiO_2 surface greatly reduced the recombination rate of charge carriers by acting as electron trapping sites due to its strong electronegativity [82].

Park and co-workers obtained a hot electron current using catalytic nanodiodes such as Pt/TiO_2 for CO oxidation [83]. This hot electron flow at the metal/oxide interface was found to be well connected with the turnover rates and selectivity of catalyzed reactions, since the local structure at the interface strongly affects the charge trapping, charge carrier dynamics, and the band structure [83]. There may be a limitation and an optimum arrangement in the design of metal/TiO_2 heterojunction to serve as highly active photocatalyst. In some instances, metal deposition can also decrease the activity of TiO_2 in photocatalytic reaction, because of the possible water reduction on Pt particles which otherwise cannot take place on the surface of pure TiO_2. Water reduction to hydrogen will consume a part of photogenerated electrons which otherwise could take part in the oxygen reduction forming reactive oxygenated species [84]. With high metal loading concentration, electron transfer from TiO_2 particles to metal can also deform the potential field in TiO_2 particles and draw a portion of holes near the metal/TiO_2 junction, which increases the recombination rate. Furthermore, it was observed that the accumulation of photoinduced electrons on the metal particles was facile, the subsequent electron transfer from the metal particles to electron acceptors may not be similarly favored. However, at higher metal loading concentrations, the electrical potential gradient is lowered and the rate of electron diffusion decreases, due to the decrease in the electron density gradient. When the two gradients are too small to increase the electron flux through the metal/TiO_2 contact, a new equilibrium is reached and hence it can be concluded that high level of metal deposition cannot enhance the charge separation and therefore the decomposition rate stops growing. The deformation of potential field in TiO_2 particles and drawing the hole near the Pt/TiO_2 junction also increases the recombination rate [84]. The deposited metal can act as shield for absorption of photons, enhance recombination at higher metal concentration and it can also activate trapped electrons. The first two processes are detrimental to photocatalytic activity, while the third process being favorable. Thus the overall activity of metal deposited titania should be considered as a result of these three competing phenomenon. The process of oxidation of deposited metal by the photogenerated hole and the reduction of metal ions by CB electrons compete with one another to decide the ultimate fate of the interface. Deposited metal can also absorb photons, but these photons are not available for the generation of charge carriers in the semiconductors, and the metal could act as a shield for TiO_2 and does not influence drastically the electron bulk mobility. Gerisher further suggested that the platinum deposits function as recombination centers [16];

$$h^+ + M^{n-} \rightarrow M^n \quad (\text{ifforexample} n = 1) \tag{3}$$

Based on geometric consideration, it is proposed that high density of small epitaxial deposits on semiconductor surface are energetically capable of trapping photoelectrons which decreases the charge carrier separation distance and thereby increasing the recombination, while small number of metal deposits may increase the interfacial charge transfer processes [16]. Furthermore, large Pt clusters acts as recombination sites due to their ability to serve as both electron/hole traps. In general, the optimization of metal deposits on TiO_2 surface for enhanced activity is often explained as the result of competition between (i) a decrease of electron–hole recombination due to the electron trapping effect by Pt clusters; (ii) electron–hole recombination on Pt. In addition to the above factors, at high concentration of metal loading, the metal deposits begin to touch and overlap with one another, thus decreasing the metal/TiO_2 interface and also decrease the efficiency of interfacial charge transfer. Ohtani et al. have pointed out that an optimal Pt loading value together with a homogeneous distribution of Pt clusters at the TiO_2 particle surface are required to enhance the photocatalytic activity [85]. In their experimental study, the authors determined an average distance between Pt clusters of ca. 10 nm.

3. Photocatalytic activity of gold deposited titania (Au/TiO_2)

Among the noble metals, gold has attracted significant interest. Gold nanoparticles have been exploited for various purposes, starting from optics and electrochemistry to environmental engineering, due to their stability, non-toxicity and biocompatibility [86]. Although gold in bulk is chemically inert toward chemisorptions of reactive molecules such as oxygen and hydrogen and has often been regarded as a poor catalyst, but however its nanosized particles are surprisingly active for many reactions [87].

It is likely that in the works of Hidalgo and co-workers the pre-sulfate treatment on TiO_2 produces a highly defective material which strengthens the adsorption of metallic species on the oxygen sites increasing the extent and effectiveness of electronic interaction between Au and TiO_2 surface [87]. Surface gold metallization would increase the charge separation and thus the efficiency of photocatalytic process. Mohapatra et al., have also found an increased activity of Au/titania catalyst prepared by using sulfate pretreated titanium oxide for the oxidation of CO at room temperature [88]. These authors attributed the higher activity to a direct interaction between sulfate ions with the gold atoms. Au/TiO_2 samples were calcined at 400 °C which still retained high amount of sulfate groups on the surface. In contrast to the works of Mohapatra et al., no sulfate species were found in samples prepared by Hidalgo et al., suggesting that different mechanisms would be operative in different reaction conditions [87,88]. The transient absorption decay measurement of Au/TiO_2 at $\lambda = 675$ nm under UV pulse illumination ($\lambda = 308$ nm) showed less intense signal compared to pure TiO_2, which was interpreted as indication of accumulation of high number of CB electrons in the Au nanoparticles [89]. In another study it was reported that the visible light induced oxidation of 2-propanol on Au/TiO_2 was initiated by SPR effect as confirmed by action spectrum analysis and they speculated that electron from Au nano particles may be injected into the TiO_2 CB and they in turn reduce the molecular oxygen adsorbed on the TiO_2 surface [90]. The resultant electron-deficient Au could oxidize organic compound to recover to its original metallic state. It was also found that the above visible light sensitive Au/TiO_2 photocatalyst oxidizes ethanol/methanol and simultaneously reduce the oxygen [91]. Many preferential or exclusive reactions are believed to proceed at the metal/oxide interface which contains sites located at atomic distances between metal atoms and the support. The local surface structure and interfacial sites is even more critical for photocatalytic processes since these sites are the loci for the transfer and subsequent trapping of photogenerated charge carriers. The interaction between a metal center and TiO_2 was found to depend on the phase composition of TiO_2 materials. Specifically, mixed phase TiO_2 appears to be different compared to single phase TiO_2 as catalyst. Kamat et al., have reported that the ratio of metal/metal ion concentration (Au^0/Au^{3+}) at the TiO_2 surface was found to dictate the process of photocatalytic oxidation of SCN^- ions at the semiconductor/metal nanocomposite [92]. The photoreduction of gold ions which readily takes place in deaerated TiO_2 suspension becomes difficult to achieve in the aerated solution. Another dominating chemical process at the TiO_2 interface is the oxidation reaction involving holes. When gold capped TiO_2 was irradiated under aerated conditions, continuous disappearance of SPR band was observed which reveals the continuous process of oxidation of metal deposits by hole. The VB holes are highly energetic to oxidize gold ($E^0 = 1.76$ V) at the interface. However, when dissolved oxygen was removed by purging N_2 gas into the system, original SPR band was restored again. It is evident from these experimental results that the metal ion reduction or metal oxidation strictly depends on the reaction medium. Most of the photocatalytic oxidation experiments reported in the literature includes dissolved oxygen as the electron scavenger. These oxygenated conditions are although effective for unmodified TiO_2 photocatalysts, such a medium may not be suitable for Au/TiO_2 nanocomposites. Thus the photogenerated hole in such composite system not only oxidizes the redox species but also oxidizes the metal deposits at the semiconductor interface. The presence of oxidized metal ion at the interface can further alter the energetics and/or act as recombination sites for photogenerated charge carriers. The increased efficiency at low concentration of $Au^0/Au^{3+} + Au^0$ on TiO_2 surface suggests that careful control of these two species at the semiconductor/metal interface is important for maximizing the performance of the photocatalysts. Although, metal ions serve as charge recombination centers, their presence along with metal should be beneficial and effective for promoting photocatalytic oxidation on a semiconductor–metal composite system. High Au^0 coverage can reduce photocatalytic activity due to the simultaneous competition for hole by both metal deposits and the substrate molecule. Further higher Au^{3+} sites serve as recombination centers [92]. Au/TiO_2 showed enhanced activity compared to Ag/TiO_2 and Pt/TiO_2 for the degradation of tartrazine [93]. It has been confirmed by several studies that the catalytic properties of metal/semiconductor heterostructure photocatalyst depends significantly on the size of deposited metal particles, the interaction between metal and TiO_2 and on the active sites on the nanostructure. The smaller metal deposits on the TiO_2 surface exhibit more negative shift of Fermi energy level. Okazaki et al. have proved by density functional studies that the adhesive energy between Au and TiO_2 for non-stoichiometric surfaces was much larger than those on stoichiometric surfaces. The charge transfer between gold and TiO_2 is more effective on non-stoichiometric Ti-rich surfaces and also on defect rich states [94]. Tian et al., have shown that interfacial electron transfer process depends on the size of Au nanoparticle on TiO_2 surface [95]. When the size of gold particles is too large, the Fermi energy level of gold particles will be lower than that of energy level of adsorbed O_2 and hence the photoelectrons cannot be energetically transferred to the adsorbed O_2. However, for quantum sized gold deposits, photoelectrons cannot be transferred from the bottom of TiO_2 CB to the gold particles since its Fermi level is much higher than the TiO_2 CB edge due to the quantum size effect. Therefore, Au particle deposits with an appropriate size that can possess an energy level between TiO_2 CB and adsorbed O_2 are very essential for the smooth transfer of the electrons [96]. The reduction of Au^{3+} ions on sulfated TiO_2 either by photodeposition or by chemical reduction methods by citrate molecules showed good activity for the phenol degradation [87b]. The samples prepared by the later

Table 3
Summary of preparation conditions and characterization results for the TiO_2 and Au/TiO_2 prepared at different light intensity.

Sample	Nominal content of Au (wt%)	Deposition time (min)	wt% Au (XRF)	Anatase crystallite size
TiO_2	0	–	0.00	21
Au/TiO_2 (high intensity: 140 W/m^2)	0.5	15	0.36	21
		120	0.45	20
	1	15	1.03	19
		120	0.82	20
	2	15	1.55	20
		120	1.56	20
Au/TiO_2 (low intensity: 0.15 W/m^2)	0.5	15	0.29	20
		30	0.29	21
		60	0.27	21
		120	0.32	19
		240	0.33	21
	1	15	0.45	21
		30	0.52	20
		60	0.54	21
		120	0.8	21
		240	0.69	20
	2	15	0.28	21
		30	0.32	21
		60	0.52	22
		120	0.77	20
		240	0.98	21

Reprinted with permission from Ref. [97] Copyright (2011) Elsevier.

Table 4
Physical properties of the photocatalytic samples, zero-order reaction rate constants (k_{app}) and initial photonic efficiency (ξ_0) of photocatalytic decomposition of oxalic acid.

Catalyst sample	Au loading pH	Method	Average metal particle (nm)	Adsorption of oxalic acid (μmol/g catalyst)	k_{app} (mmol/Lmin)	ξ_0 (%)
None	–	–	–	–	No	–
TiO_2	–	–	–	850	0.028	0.76
1%Au/TiO_2	3	PR	18	590	0.02	0.79
1%Au/TiO_2	5	PR	9	500	0.055	1.49
1%Au/TiO_2	7	PR	5	430	0.069	1.87
1%Au/TiO_2	9	PR	4	450	0062	1.68
1%Au/TiO_2	7	PD	5	440	0.064	1.74

Reprinted with permission from Ref. [103] Copyright (2007) Elsevier.
The gold was loaded on TiO_2 by the photoreduction method (PR) and deposition–precipitation method (PD).

method showed improved performance. Compared to the photodeposition method, chemical reduction method by citrate molecules gave much homogeneous and smaller gold deposits with better dispersion which resulted in stronger bonding and superior electronic junction between gold nano particles and the TiO_2 surface. Au/TiO_2 prepared by photodeposition method using a low intensity light illumination (0.14 W/m^2 UVA range) showed notable improvement in photocatalytic activity for the phenol decomposition under UV light compared to Au/TiO_2 prepared by the same method using high intensity illumination (140 W/m^2 UVA range) [97]. The poor activity of the later sample was due to the production of very large and heterogeneously distributed gold deposits which serve as recombination centers rather than as the trap sites for photogenerated electrons (Table 3). The extent of gold deposition, aggregation and oxidation state of Au can be controlled effectively by changing the deposition time for Au/TiO_2 (prepared at low intensity light illumination) [97]. Au deposited on Ti^{3+} self doped TiO_2 effectively boosted the photocatalytic degradation of Rhodamine B (RhB) [98].

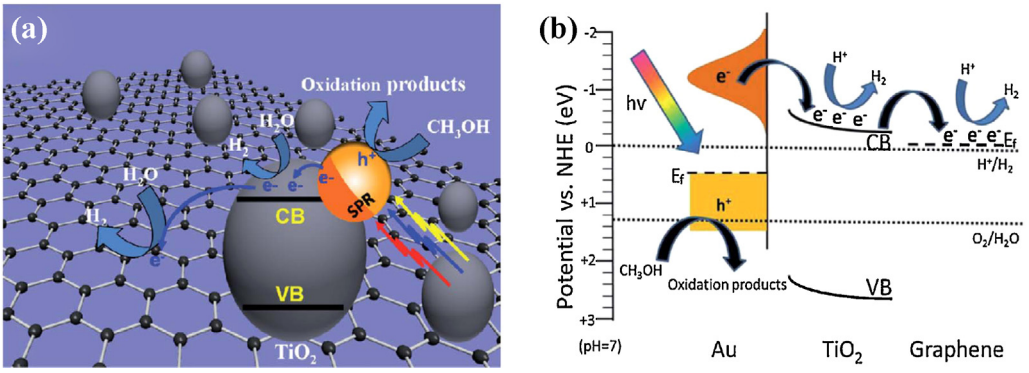

Fig. 5. (a) Schematic diagram of Au/TiO_2/graphene composite and (b) illustration of energy band structure and charge carrier transfer and separation in the Au/TiO_2/graphene composite for photocatalytic H_2-production under visible light irradiation.
Reprinted with permission from Ref. [104] Copyright (2014) Royal Society of Chemistry.

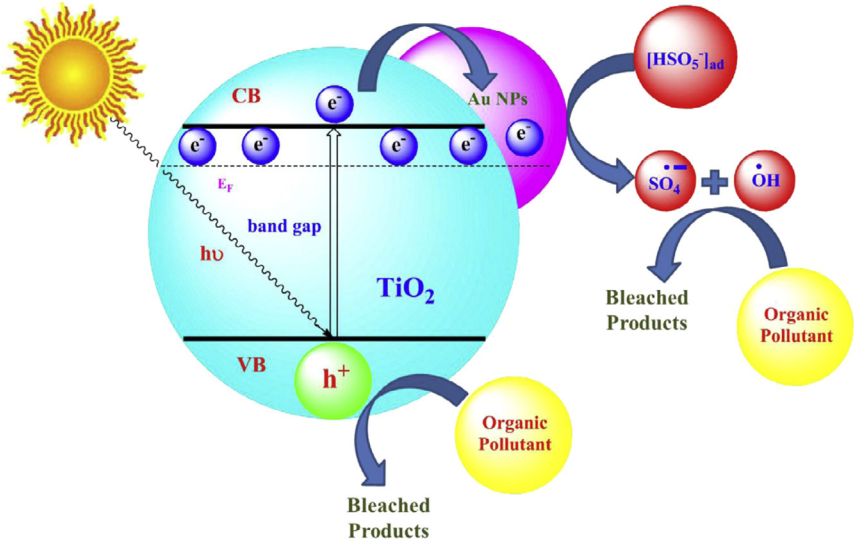

Fig. 6. Proposed mechanism for the activation of PMS in the presence of Au/TiO_2 nanoparticles.
Reprinted with permission from Ref. [111] Copyright (2014) Elsevier.

The defect mediated TiO_2 was synthesized by using TiH_2 as precursor and the noble metal was directly deposited onto the surface of defective titania through the in situ redox reaction between the noble metal and the reductive Ti^{3+}species. In non-stoichiometric TiO_2 the presence of large amount of oxygen vacancies substantially shifts the VB maximum to form a tail band. This tail band along with large number of oxygen vacancies concomitantly hybridizes with Ti^{3+} can form a new band just below the CB minimum. These two defect states eventually narrowed the bandgap of pristine TiO_2 and rendered visible light response. The potential of Ti^{3+} is thermodynamically more negative (~0.12–0.3 V below the CB minimum) than the highly oxidative noble metal ions. When $HAuCl_4$ solution is introduced into the reaction mixture, Ti^{3+} on the surface can immediately reduce the Au^{3+} species into metallic Au nanoparticles accompanied by the simultaneous oxidation of Ti^{3+} ions into Ti^{4+} state resulting in Au/TiO_2 nanocomposites [99]. This direct in situ reduction involves no foreign additives and thus makes intimate contact between metal/TiO_2 interfaces [98]. TiO_2 surface modified with Au25 clusters exhibited enhancement in the oxidation reactions of phenol derivates and also ferrocyanide [100]. It can also show reduction reactions of Ag^+, Cu^{2+} and dissolved oxygen. A thermodynamically uphill reaction such as oxidation of phenol accompanied by reduction of Cu^{2+} is also driven by this catalyst under the irradiation of light with wavelength of 860 nm [100]. Au/TiO_2 demonstrated enhanced photocatalytic decomposition of MO under visible light exposure while the activity was reduced under UV light which was attributed to the decrease in the TiO_2 surface area by Au deposits [101]. Finite-difference time-domain simulations of these Au nanoparticles on TiO_2 photocatalyst show that the enhanced photocatalytic activity is due to the large plasmonic enhancement of the incident electromagnetic field, which increases the rate of electron–hole pair generation at the TiO_2 surface resulting in the enhancement of MO photodecomposition. This enhancement mechanism relies on the presence of defect states in the TiO_2, which enabled sub-bandgap absorption [102]. The rate of photocatalytic destruction of oxalic acid increased with TiO_2 modified with Au nanoparticles in comparison to the pure TiO_2 [103]. Remarkable influence of the pH on the particle size of Au was observed by photoreduction method. The dimensions of the gold nanoparticles on the TiO_2 surface decreased with increasing the pH of the medium. The photocatalytic activity of Au/TiO_2 sample obtained at pH 3 did not show any improved activity when compared to DP25 due to smaller number of gold nanosized particles on the surface of the photocatalyst. The size of Au nanoparticle decreases in the photoreduction method by increasing the pH of the medium containing gold salt solution with TiO_2 which results in improvement of the photocatalytic activity (Table 4). At pH 9 fast precipitation of $Au(OH)_nCl_{4-n}$ takes place and further the reduced gold is not deposited on the TiO_2 surface [103]. With the increase in the number of metal nanoparticle serving as effective electron traps, the photocatalytic activity increases only to a certain extent. But however further increase in the number of metal nanoparticles band-gap excitation of TiO_2 is hampered and decreases the extent of adsorption of oxalic acid and also water due to the large surface coverage by Au nanoparticles [103]. Microwave assisted hydrothermal synthesis of graphene based Au/TiO_2 (Au = 0.25 wt%) showed enhanced photocatalytic hydrogen evolution under visible light irradiation when compared to TiO_2, graphene–TiO_2 and graphene–Au [104]. Au is excited at 420 nm due to plasmonic resonance and the charge separation takes place by the transfer of electrons from Au to TiO_2 CB which in turn tends to get transferred into graphene sheets as the redox potential of the redox couple (graphene/graphene$^-$) is −0.08 eV which is lower than TiO_2 CB (−0.24 eV) [105]. The mobility of these electrons in the graphene sheets is high which led to the retardation of charge carrier recombination and suppressed the reverse reaction by separating the evolution sites of hydrogen and oxygen (Fig. 5). The Fermi level of Au is around 0.6 eV lower than TiO_2 CB [106]. There is a potential energy barrier of magnitude ~1 eV (Schottky barrier) at the interface between Au and TiO_2 which will hinder the process of electron injection from Au to TiO_2 on SPR excitation [107]. Under visible light irradiation the Au would give rise to SPR effect which leads to the intraband excitation, generating energetic electrons whose energy is above 1.0 eV with respect to the Fermi level of Au which would overcome the Schottky barrier leading to the transfer of electrons to TiO_2 CB. In addition graphene is an excellent electron acceptor with a superior conductivity due to its two dimensional π conjunction structure serving as electron collector and transporter in the graphene/Au/TiO_2 composite [108]. The observed hydrogen production enhancement was further confirmed by transient photocurrent response and electrochemical impedance spectroscopy (EIS) experiments [104]. Au/N–TiO_2 showed better photocatalytic degradation of oxalic acid under various light sources like only UV, only visible and the mixture of UV-visible light irradiation compared to N–TiO_2, Au/TiO_2 and TiO_2 due to the dominating influence of charge separation [109]. The longer lifetime of the photoexcited

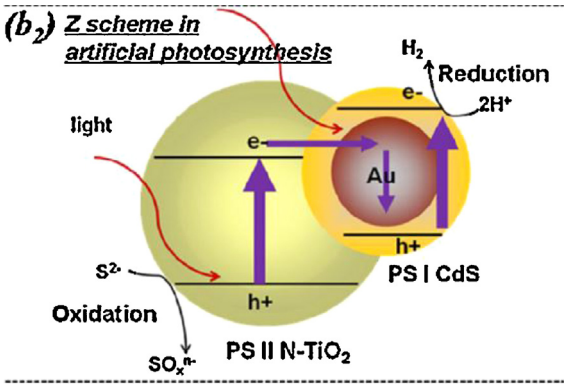

Fig. 7. Z-scheme in CdS/Au/N–TiO_2 composite representing artificial photosynthesis.

Reprinted with permission from Ref. [116] Copyright (2014) Elsevier.

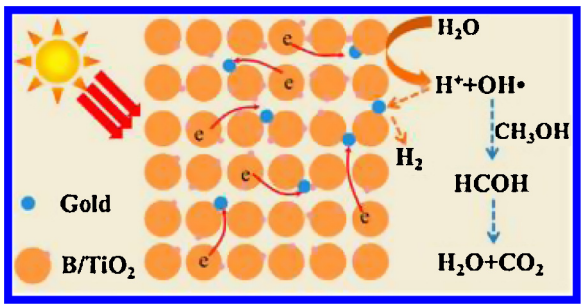

Fig. 8. The proposed reaction pathway of photocatalytic hydrogen generation from water/methanol suspension containing Au/B–TiO_2 catalyst.

Reprinted with permission from Ref. [120] Copyright (2014) American Chemical Society.

electron in the TiO_2 CB results in the accumulation of electrons on Au nanoparticles and to the formation of new quasi-Fermi level favoring the formation of hydroxyl radical and superoxide radicals [110]. The interaction of highly reactive hydroxyl radicals with oxalic acid leads to total destruction. Au/TiO_2 prepared by deposition–precipitation method by virtue of its visible light absorption property and rapid charge separation at the interface showed excellent photocatalytic property toward the degradation of ceftiofur sodium (CFS) a third generation cephalosporin antibiotic under UV–visible light irradiation [111]. Under illumination conditions the CB electrons are attracted by Au nanoparticles owing to the difference in the work function between Au and TiO_2 and these electrons are driven by an electric field and hence the light induced charge separation becomes easier (Fig. 6). TEM images showed that the Au particles were highly dispersed on TiO_2 with a condensed shape having a large interfacial area as a result of low interfacial energy between gold and TiO_2 [112]. The photocatalytic degradation experiments in presence of oxidants like peroxomonosulfate, peroxodisulfate and hydrogen peroxide increased the degradation rate and the activity is attributed to the immediate trapping of the photogenerated electrons by the oxidants that lead to the decrease in charge recombination [111]. Au/N–TiO_2//N–WO_3 (4% WO_3 optimum concentration) exhibited enhanced photocatalytic oxidation of aqueous 2,4,6-trinitrotoluene (TNT) under UV and visible light irradiation when compared to other samples [113]. This enhanced activity was a result of more efficient charge separation which led to the increase in lifetime of charge carriers and enhanced the efficiency of interfacial charge transfer to adsorbed substrates. In addition gold nanoparticles served as effective traps for electrons due to the formation of a Schottky barrier at the metal–semiconductor contact. The photonic efficiency of N–TiO_2 and coupled N–WO_3/N–TiO_2 is much higher than the efficiency of TiO_2 under visible light irradiation due to the substitution of nitrogen atoms (1.2 at%) into the crystal lattice of TiO_2 and WO_3 photocatalysts which led to the band gap narrowing owing to the formation of a new impurity level [114]. The noble metal–TiO_2 core–shell structure (M@TiO_2) has been designed as a promising strategy because the metal cores are protected by the TiO_2 shell, which is chemically inert, stable and also exhibits better durability [115]. A three component heterostructures CdS(Shell)/Au(core)/N–TiO_2 exhibited enhanced hydrogen evolution rates which was about 2.6 times greater than N–TiO_2 (under UV/visible light irradiation) and about 270 times greater than Au/N–TiO_2 (under visible light irradiation) [116]. The unique architecture-hierarchical macro/mesoporous morphology as observed in the natural leaves for photosynthesis is retained in CdS/Au/N–TiO_2 with an enhanced overall light harvesting ability and offered more reaction sites for adsorption in the catalytic reactions. The photogenerated electrons in the N–TiO_2 CB photosystem II (PS II) can easily flow into Au through the Schottky barrier and the holes in the VB are available for the oxidation reaction [117,118]. Simultaneously the holes in the VB of CdS photosystem I (PS I) will also easily flow into Au to combine with the stored electrons because of higher Fermi energy level when compared to CdS and the electrons left in the CdS CB are available for the reduction reaction. Thus the resulted vectorial electron transfer from N–TiO_2 to Au to CdS realizes the complete separation of holes in N–TiO_2 VB and the electrons in the CdS CB (Fig. 7). Furthermore the electron supply from N–TiO_2 to CdS via Au restricts the self decomposition of CdS due to the oxidation of surface S^{2-} ions by the VB holes of CdS [119]. The TEM images suggested that the sizes and distribution of Au nanoparticles on N–TiO_2 was controlled by changing the irradiation time, irradiation distance and the concentration of methanol in $HAuCl_4$ solution. At relatively high concentration of methanol the Au particles preferred to cluster together and the particle distribution was not homogeneous. Many particles were agglomerated indicating that these particles nucleated in solution. The sacrificial agent raises the charge carrier concentration in the nanoparticle. In the meantime with the increase in the irradiation time, the average diameter of Au deposit increases. The fabrication of this system was based on biological morphology which provided a proof for the bio-inspired design of artificial photosynthetic system for enhanced photocatalytic performance [116]. Au/B–TiO_2 synthesized by sol gel hydrothermal method promoted a remarkable enhancement in hydrogen evolution from water/methanol mixture under visible light irradiation [120]. The formation of Ti–O–B structure provides vacancies or microvoids for gold ions which were converted into metallic gold after calcination as revealed by NMR studies [121,122]. These embedded gold particles which are present in close proximity to B–TiO_2 act as efficient electron sinks and prolong the lifetime of charge carriers thereby enhancing the activity (Fig. 8). The electrons are easily transferred from TiO_2 to Au while the holes in the VB migrate to TiO_2 surface and react with adsorbed water to form hydroxyl radicals and hydrogen ion. Meanwhile these radicals would attack the methanol molecules and oxidize them into formaldehyde which is further oxidized to CO_2 and water. The trapped electrons on the gold nanoparticles facilitate the reduction of H^+ ions into hydrogen. For the first time, the isotopic tracer studies using a gas chromatograph isotope ratio mass spectrometer along with a series of control experiments revealed that the produced hydrogen was originated mainly from water rather than methanol, whereas the direct oxidation of methanol did not lead to hydrogen generation [120].

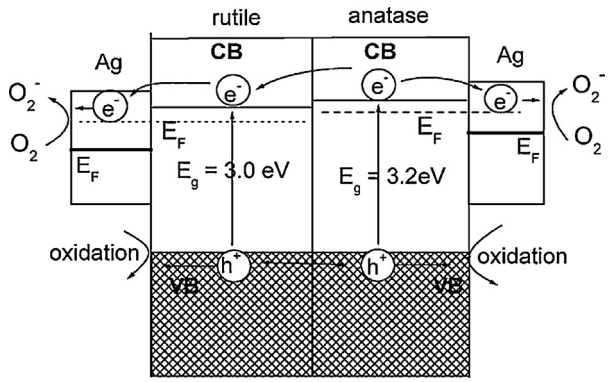

Fig. 9. Interface charge-carrier transfer dynamics of anatase/rutile, Ag/anatase and Ag/rutile within Ag/TiO_2 composite thin films.
Reprinted with permission from Ref. [124a] Copyright (2005) Elsevier.

4. Photocatalytic activity of silver deposited titania (Ag/TiO_2)

The Ag noble metal is a promising candidate for extensive application because of its low cost, inherent antibacterial activity and can be adopted by facile preparation techniques [123]. Ag/TiO_2 multiphase nanocomposite thin films were prepared on quartz substrates by liquid phase deposition method from a mixed aqueous solution of ammonium hexafluorotitanate, silver nitrate and boric acid under ambient temperature and atmosphere followed by calcination at 500 °C for 1 h. This catalyst showed enhanced photocatalytic activity for the degradation of MO under UV light [124]. PXRD results suggested that the grain growth of anatase was suppressed upon Ag^+ adsorption at 0.02 M concentration of $AgNO_3$ [124,125]. Phase transformation from anatase to brookite was catalyzed by Ag^+ ions when $AgNO_3$ concentration is ≥0.02 M. Further increase of $AgNO_3$ concentration from 0.02 to 0.03 M leads to the rutile phase formation along with the presence of metallic Ag on the surface [126]. The phase transformation temperature of anatase to rutile in this case was greatly decreased by the silver metallization due to the following reasons: (i) the grain size of anatase crystallites were reduced by the presence of $AgNO_3$; (ii) total grain boundary energy is increased and (iii) the thermal decomposition of $AgNO_3$ produced intensive exothermic heat which was sufficient enough to cause phase transformation. The presence of Ag in the thin films produced a Schottky barrier, which facilitated the electron capture. A significant improvement of photocatalytic activity was observed when $AgNO_3$ concentration is around 0.03–0.05 M due to the following causes: (i) the catalyst sample consisted of anatase, brookite, rutile phases of TiO_2 along with metallic Ag suggesting that the films contained many heterojunctions such as anatase/rutile, anatase/brookite and rutile/brookite phases. The interface between the two phases served as a rapid separation site for the photogenerated charge carriers due to the difference in the energy levels of their CB and VB edge positions; (ii) metal/semiconductor hetero-junctions such as Ag/anatase, Ag/rutile and Ag/brookite also existed in the films due to the Ag deposition (Fig. 9). The coupling between Ag/anatase and Ag/rutile allowed the electron migration from anatase or rutile phases to Ag metal deposits. This electron transfer process significantly retards the recombination of charge carriers in both anatase and rutile phases and (iii) on UV light excitation, electrons gets accumulated either in the metallic Ag deposits or in the low lying CB of rutile, whereas holes could get accumulated in the VB of both anatase and rutile due to similar VB edge positions. The accumulated electrons from Ag deposits or from the CB of rutile could easily be transferred to surface adsorbed oxygen to form O_2^- or O_2^{2-} [127]. Contrarily in another study the deposition of Ag on the surface of P25 containing both anatase and rutile phases had negligible effect on the degradation of aspartic acid, while reaction rate was quite high with either anatase or rutile individually [128]. C/Ag/TiO_2 microspheres synthesized via controlled hydrolysis of tetrabutyl titanate in ethanol medium and followed by calcination process using $AgNO_3$ as Ag source and citric acid as carbon source showed an enhanced the photocatalytic activity for RhB degradation under UV as well as visible light region compared to pristine TiO_2 and Ag/TiO_2 [129]. The addition of citric acid to the system largely increased the Ag density due to its reductive property and it can also induce the disorderness of sp^2 orbitals of carbon during the heat treatment (500 °C for 2 h) which gets coated on TiO_2 surface. Raman spectra of C/Ag/TiO_2 showed two bands around 1354 and 1594 cm^{-1} attributed to the distorted sp^2 carbon and well ordered graphite like structure on the TiO_2 surface. These results suggested that sp^2 hybrid orbitals of carbon interacts with orbitals of silver nanoparticles to increase the SPR effect of Ag and also enhances the light absorption ability of C/Ag/TiO_2 both under UV and visible light [130].

Horavath et al. reported that the process of photoreduction of silver ions on the TiO_2 surface was not influenced by the presence of oxygen in the system [131]. This fact was confirmed by the experiment carried out by bubbling Ar to replace oxygen in the reaction mixture and also by the use of catalyst prepared under Ar atmosphere. Both experiments displayed almost similar results [131]. It means that electron scavenging by the oxygen molecules at the surface of the excited TiO_2 cannot efficiently compete with the electron transfer process to the metallic silver. When Ag/TiO_2 nanocomposite was used in the dye degradation reaction, photoexcited electrons were found to get readily transferred from TiO_2 to metal nanoparticles, but their subsequent release to the dye molecules occurred only via the smaller metal nanoparticles [132]. The photocatalytic performance of metal/TiO_2 heterojunction is a strong function of size and shape of the metal nanoclusters. Christopher reported that by changing the size and shape of Ag nanocluster it is possible to maximize photochemical activity of semiconductor at a given excitation wavelength [133]. There are number of physical mechanisms previously observed that could potentially explain the enhanced photocatalytic activity of the composite system compared to pure titania; (i) electron transfer from TiO_2 to Ag nanoparticles effectively increases the life time of electron–hole pairs; (ii) electron transfer from Ag to TiO_2 is mediated by Ag surface plasmons under visible light irradiation; (iii) the localized heating of Ag nanostructures due to non-radiative decay converts the Ag surface plasmons into phonon modes; (iv) indirect transfer of photons from Ag nanoparticles to TiO_2 via radiative decay of surface plasmon states to excite electrons in TiO_2 results in the increase of electron–hole pair concentration. However, Christopher ruled out (i)–(iii) mechanism and suggested that pathway (iv) is highly responsible for enhanced activity for Ag nanocube/TiO_2 compared to Ag nanospheres (75 ± 13 nm diameter)/TiO_2 and Ag nanowire (70 ± 12 nm diameter)/TiO_2 system for the degradation of MB. The presence of Ag deposits on the TiO_2 surface enhanced the photo oxidation of oxalic acid by a factor of 5 times. The accumulation of electrons in the nanosize silver particle increases the probability of formation of excited oxygen atoms by the process of electron transfer from O_{ads}^- which itself was originated from the electron donation by $O_2^{2-}{}_{ads}$ to the hole [131]. Highly ordered TiO_2 nanotube arrays decorated with Ag nanoparticles prepared by a direct electrodeposition method (at −0.6 V for 60 s) exhibited enhanced activity for MO photodegradation under UV/visible light irradiation [134]. On increasing the deposition time, the size and the concentration of Ag increased on the TiO_2 surface [135]. When the deposition time was varied as 20, 60, 90 s, the average size of Ag deposit was found to be ~5.7 (2 at%), ~9.6 (6 at%) and ~12.2 nm (9 at%), respectively. According to Chen et al., when the

radius of the Ag nano deposit was less than that of 30 nm, strong absorption in the visible light was observed [136]. Thus the photogenerated electrons excited by decaying surface plasmon can occupy the empty states in the excited state of Ag. These excited electrons migrate from the excited state of Ag to the TiO_2 CB leading to the enhanced photocatalytic activity [137]. Devi et al., has reported the enhanced *E. coli* (a gram negative bacteria) bactericidal activity of Ag (0.10%)/TiO_2 under solar light and the activity of the catalyst was attributed to the SPR effect of Ag nanoparticles which creates an enhanced local electric field on the surface of TiO_2 [13]. The photogenerated reactive oxygen species (ROS) such as $^{\bullet}OH$ and H_2O_2 attacks the polyunsaturated phospholipids in lipid peroxidation reaction which causes the breakdown of its cell membrane structure and also destructs its associated functions. The effect of the EROS (Externally generated Reactive Oxygen Species) and IROS (Internally generated Reactive Oxygen Species within the bacteria) on the bactericidal inactivation was correlated with each other. These ROS target the cell components like DNA, RNA, proteins and lipids. The IROS produced within the cell will have detrimental effect on *E. coli* but the enzymes like catalase and superoxide dismutase converts IROS into O_2 and water. The EROS comes in contact with the bacteria and directly attacks the polyunsaturated fatty acids in membranes and initiates lipid peroxidation and disrupts the function of the above enzymes. The mechanism of the cell death is due to the lipid peroxidation reaction that subsequently causes a breakdown of the cell membrane structure and their associated functions, leading to the simultaneous loss of cell viability [18]. Similar research using Ag/TiO_2 nanotube arrays with 100 nm length exhibited enhanced antibacterial activity for the destruction of *E. coli* and *S. aureus* both in dark and UV light irradiation, respectively [138]. The hydroxyl radical and superoxide radicals generated during photoexcitation can damage the stereostructure of the active enzyme and block the DNA of microorganisms resulting in inactivity of enzymes and dysfunction or destruction of the cell wall or plasma membrane by binding with their proteins especially with enzymes [186]. The positive antibacterial behavior under UV light is a synergistic effect between nano Ag and TiO_2. In the dark, nano Ag plays an active role in antibacterial behavior and TiO_2 nanotubes serve as good carrier support for nano Ag [139]. Therefore Ag/TiO_2 nanotube arrays suited well for endo-prosthetic applications due to their excellent antibacterial activities in the dark. The highly ordered and smooth Ag/TiO_2 nanotubes array with one directional electric channel for electron transportation showed enhanced photoconversion efficiency and hydrogen evolution rate under UV light irradiation [140]. The ordered and smooth architecture enhances the specific surface area. Ag decorated titania of both nanorod array (NRA) and nanopore array (NPA) designed as Surface-Enhanced Raman Scattering (SERS) active substrate is used for a sensitive detection application [141]. NRA of TiO_2 was grown on glass slide by hydrothermal synthesis process. NPA of TiO_2 was grown on the titanium sheet by a two-step anodization process. Silver deposition on the surface of NRA and NPA was performed by electroless deposition method. Ag/TiO_2 NRA had smaller silver interparticle gaps and more hot-spots than Ag/TiO_2 NPA, exhibiting a higher SERS activity. The analytical enhancement factor was higher for Ag/TiO_2 NRA (7.8×10^5) compared to Ag/TiO_2 NPA (1.8×10^5). Further, Ag/TiO_2 NRA substrate could even detect a very low concentration of 4-mercaptobenzoic acid (5×10^{-12} M) when used as a probe molecule, showing a sensitive SERS detection performance. In addition, Ag/TiO_2 NRA also exhibited photocatalytic decomposition of these adsorbed organic molecules to recover a clean surface under UV irradiation, exhibiting a self-cleaning activity [141]. In another research study Ag/TiO_2 nanocomposite exhibited much higher photocatalytic activity than bare TiO_2 for the degradation of rhodamine 6G (R6G) and MB molecules under UV light [142]. This photocatalyst served as a high sensitive SERS substrate for in situ monitoring of the photocatalytic decomposition reaction and the catalyst is recyclable with its self cleaning function. Full wave numerical calculations revealed that the improved photocatalysis and SERS efficiencies were attributed to the largely enhanced electromagnetic near field in the nanocomposites. This present study stimulates the development of synthetic approaches of other one dimensional nanocomposite materials with improved properties and multiple functionalities [142]. Ag/TiO_2 nanotubes with dimensions of 200 mm length and 50 nm diameter were fabricated by electrochemical anodization of Ti substrate on which Ag nanoparticles were deposited by a silver mirror reaction [143]. This Ag/TiO_2 nanotubes exhibited highest antibacterial activity for *E. coli* inactivation under UV light illumination. Their study suggested that antibacterial activity was independent of the length of the nanotube but was dependent on its diameter. In addition anatase nanotube showed the highest antibacterial activity compared to rutile and amorphous titania. Hydrolysis of silver ions in the silver mirror reaction is one of the factor which influences the activity of Ag/TiO_2 [144]. Ag deposited on the TiO_2 nanotube can accelerate the process of hydrolysis due to its large specific surface area and it can release higher number of silver ions within a given time period compared to the catalyst in which silver is deposited on the polished titanium plates.

Ag/TiO_2 nanoplate arrays grown on activated carbon fiber showed enhanced photocatalytic degradation of MB under both UV/visible light irradiation [145]. Ag was deposited by photodeposition method and optimum UV light irradiation time for the process of Ag deposition was found to be 10 min. The concentration of the deposited Ag increases with the increase in the deposition time. The increased Ag amount would prevent or hinder the contact between TiO_2 and the pollutant MB molecule and it also decreases the number of photons absorbed [146]. Ag nanoparticles with Fermi level (E_f) located around 0.4 V are found to be good electron acceptors and act as efficient electron traps under UV irradiation [147]. These electrons react with adsorbed oxygen to form superoxide radicals [148]. In addition holes at TiO_2 VB lead to the production of hydroxyl radical under UV/visible light irradiation. Under visible light irradiation most of the hot electrons are excited from the surface of Ag due to the SPR effect and are transferred to TiO_2 CB which then diffuses to the surrounding medium to degrade MB molecules [149]. Wet chemistry immobilization of plasmonic Ag nanoparticles on the surface of P25 TiO_2 through a bifunctional linker molecule such as 3-mercaptopropionic acid showed enhanced photocatalytic degradation of Alizarin Red S under UV/visible light irradiation compared to unmodified P25 and the enhanced activity is attributed to the formation of Schottky barrier leading to efficient charge separation [150]. The photodegradation experiments in the visible light irradiation inferred that the P25 bicrystalline photosensitization process is dominant for both Ag/P25 and P25 catalyst at the beginning of the degradation reaction and it was found that Ag nanoparticles did not have any prominent role at this stage of the reaction. However after the initialization, bicrystalline photosensitization effect is diminished and it was possible to observe the effect of the local excitation of the photocatalyst through SPR effect [150]. In another study porous TiO_2 sheets obtained by aqueous tape casting method further modified with Ag deposition showed enhanced MO degradation under UV light illumination compared to bare TiO_2 sheets. The deposited Ag particles served as electron traps to hinder charge carrier recombination [151]. TiO_2 nanoparticles synthesized via in situ sol–gel method followed by Ag deposition via reduction method with dextrose as reductant and sodium dodecyl sulfate as stabilizer exhibited excellent reduction of 4-nitrophenol to 4-aminophenol at room temperature suggesting the commercial exploitation of heterogeneous catalyst for the reduction of nitrocompounds [152]. Ag/TiO_2

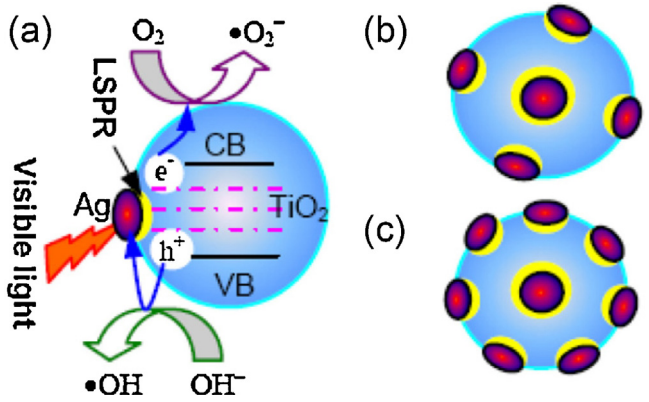

Fig. 10. A photocatalytic mechanisms for the plasmonic Ag@P25 photocatalysts. Reprinted with permission from Ref. [157] Copyright (2013) Elsevier.

with Ag > 0.5 wt% exhibited significant efficiency for the degradation of amoxicillin and 2,4-dichlorophenol (endocrine disturbing compounds) under artificial solar light when compared to TiO_2 [153]. This notable improvement was attributed by the unique characteristics of Ag SPR effect which enabled Ag to absorb light in the visible spectrum. The charge density is redistributed and thus establishes a strong coulombic restoring force which results in the oscillation of charge density. The in phase oscillations (with the incident light) in this case can be compared to simple harmonic oscillator [154]. Further, these charge density oscillations decreased the dielectric constant of the surrounding matrix [155]. TiO_2 nanotube films prepared by using NH_4F (0.25 mol/L) and 9:1 volume ratio of glycerol to water under the conditions of 25 V oxidation voltage (for 2 h anodic oxidation time) had excellent structural integrity, an ordered arrangement, large diameters and thin walls [156]. Further, Ag metallization on the above TiO_2 nanotubes was done by using ultrasonic atomization-UV photo reduction method and this Ag/TiO_2 nanotube films showed good activity for acetic acid decomposition under UV light irradiation. A mathematical model for catalytic degradation was established based on a hyperbolic model [156].

$$\frac{-\mathrm{dC(HAc)}_t}{\mathrm{dt}} = \frac{\mathrm{C(HAc)}_t^2}{a\,\mathrm{C(HAc)}_0} \quad (4)$$

$C(HAc)_t$ is acetic acid concentration at degradation time t, $C(HAc)_0$ is the initial acetic acid concentration and a is concentration factor ($a = f(C)$). The plot of reciprocal of degradation rate versus $1/t$ gave the value of $a = 0.113\,C(HAc)_0 + 0.435$.

1%Ag@TiO_2 (P25) nanocrystals showed remarkable photocatalytic activity for the photodegradation of RhB under visible light irradiation [157]. This catalyst was synthesized by in situ photoreduction of Ag^+ ion on TiO_2 in polyvinylpyrrolidine (PVP)–ethanol suspensions. The Ag nanocrystals of 1–3 nm size was deposited on the surface of TiO_2 (20–30 nm) to form a non-centrosymmetric Ag@TiO_2 nanostructures with abundant Ag/TiO_2 interfaces. This results in different dielectric environments surrounding the plasmonic Ag (TiO_2 with higher refractive index on one side and RhB solution with lower refractive index on the other side). Excitation of SPR occurs on visible light irradiation resulting in strong localized plasmonic near fields close to Ag/TiO_2 interface (Fig. 10). These surface plasmon excitations leads to the generation of electron–hole pairs via optical transitions between localized electronic states in the band gap of TiO_2 [158]. At low Ag (0.5%) loading density, the photocatalytic activity decreased since the Ag/TiO_2 interface is not quite large enough for efficient visible light absorption. Even at higher Ag loading density the activity decreased as the adjacent visible light induced plasmonic near fields regions are too close and easily overlap with each other facilitating the recombination of photogenerated charge carriers. Therefore optimum Ag loading facilitates visible light absorption and also has high separation efficiency of charge carriers [157,158]. Nanostructured Ag/TiO_2 hybrid nanofibers prepared via a simple electrospinning process combined with silver mirror reaction exhibited enhanced photocatalytic activity for the degradation of RhB under simulated sunlight irradiation. This activity was attributed to several factors like high dispersion of Ag nanoparticles on individual TiO_2 nanofibers, preferable adsorption behavior of RhB molecules and the synergistic function between the dispersed networks with quantum size effect of Ag/TiO_2 nanofibers [159]. It is also proved that a proper silver mirror reaction time (15 min) will result in an optimal photocatalytic effect (Table 5). Any excess and redundant Ag will be disadvantageous for catalytic activity because of the excessive occupation of the active sites on the TiO_2 nanostructures [159]. Ag/TiO_2 and TiO_2 film coatings deposited using sol gel coating method showed higher photocatalytic activity for bisphenol-A degradation compared to the similar coatings prepared by using magnetron sputtering method [160]. This difference is caused by smaller Ag grain sizes as obtained from the sol–gel derived coatings when compared to the magnetron coatings. Hydroxyapatite modified Ag/TiO_2 exhibited better photocatalytic activity for acetone degradation under visible light irradiation when compared to Ag/TiO_2, TiO_2 and P25 [161]. Hydroxyapatite [$Ca_{10}(PO_4)_6(OH)_2$] possess excellent adsorption capacity as well as biocompatibility [162].

Table 5
Ag (wt%):Ti(wt%) of Ag/TiO_2 samples prepared by simple electrospinning process combined with silver mirror.

Sample number	Silver mirror reaction time (min)	Ag(wt%):Ti(wt%)
1	5	1:15.98
2	15	1:2.82
3	30	1.43:1

Reprinted with permission from Ref. [159] Copyright (2013) Elsevier.

The dye sensitized solar cells (DSSC) fabricated with Ag/N–TiO_2 showed an enhanced solar to electrical energy conversion efficiency of 8.15% compared to DSSC composed of unmodified TiO_2 which shows 2.19% conversion efficiency under simulated solar irradiation of 100 mW cm^{-2} with AM 1.5 G [163]. The improvement was mainly attributed to Ag deposition and incorporation of nitrogen into TiO_2 lattice in the form of N–Ti–O which partially converts Ti^{4+} ions to Ti^{3+} ions effectively contributing toward visible light absorption [164]. Under light illumination conditions the dye N719 absorbs incident light and promotes electrons to the excited state which are injected into Ag nanoparticles and these excited electrons are in turn transferred to TiO_2 CB [165,166]. The dye N719 cation is then oxidized by receiving electrons from the electrolyte through the redox system. The electrons through the external circuit are available at the counter Pt electrode to regenerate electrolyte. In this case Ag deposits served as electron sink, acts as scattering element for plasmonic scattering, can also trap the photon and it also enhances the near field (Fig. 11). In addition the accumulation of electrons on Ag deposits shifts the position of its Fermi level closer to TiO_2 CB. The excited electrons from TiO_2 CB (transferred from Ag deposits), were collected by indium tin oxide (ITO) acting as current collector thus improving the photocurrent and photovoltaic performance under the visible light region [167]. Ag/N–TiO_2 nanotube arrays fabricated via electrodeposition method at deposition potential of −1.0 V with deposition time of 5 s showed enhanced photodegradation of acid orange II compared to TiO_2 and N–TiO_2 [168]. The photocurrent density of Ag/N–TiO_2 (150 μA/cm^2) was found to be highest when compared to other samples under visible light. The zero-current potential

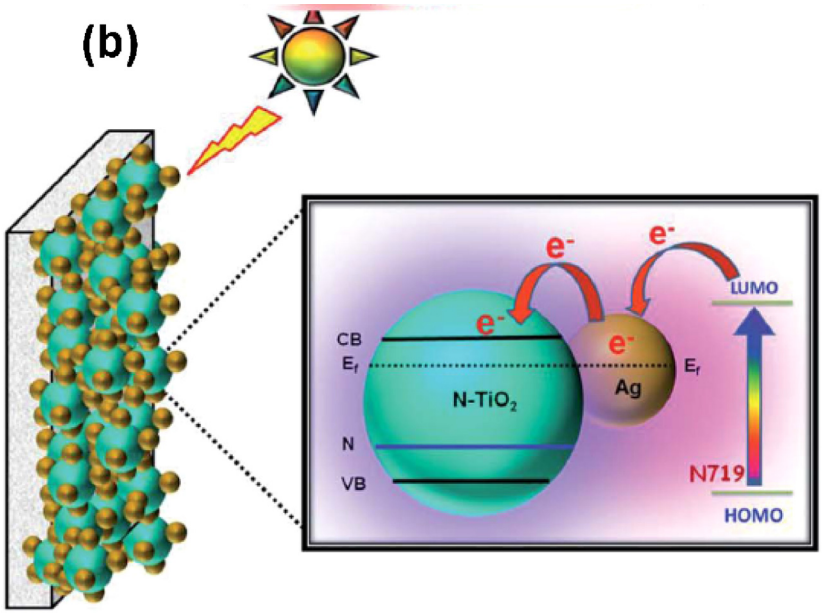

Fig. 11. Charge transfer mechanism for Ag/N–TiO_2 photoanode-modified DSSC.
Reprinted with permission from Ref. [163] Copyright (2014) Royal Society of Chemistry.

(E_{zcp}) for Ag/N–TiO_2 and TiO_2 nanotube arrays was found to be −0.768 V and −0.607 V versus Ag/AgCl, respectively. This negative shift of potential by 0.161 V was ascribed to the modification of TiO_2 by nitrogen doping and Ag deposition suggesting that Ag/N–TiO_2 photocatalyst needs a lower potential (less energy) to extract the photoinduced electrons to the external circuit [168]. Ag/N–TiO_2 coated with PVP a non-conducting organic stabilizer exhibited enhanced H_2 evolution and high photocurrent efficiency under visible light irradiation when compared to N–TiO_2 and Au/N–TiO_2. The activity was attributed to the formation of intense electric fields at the Ag particle surface which increases the rate of formation of electron–hole pairs near the N–TiO_2 particle surface [169]. The advantages of forming charge carrier pairs near the semiconductor surface rather than in the bulk are as follows: (i) the charge carriers are readily separated from each other under the influence of the surface potential and (ii) the charge carriers have a shorter distance to migrate in order to reach the surface, where they can take part in photocatalytic transformation reactions. This effectively means that the probability of photoreaction is enhanced relative to the probability of charge-carrier recombination. The optimal distance between a semiconductor and plasmonic nanostructure is affected by Forster energy transfer from the semiconductor to the metal [170]. In the photoelectrodes, the organic PVP layer acts as the buffer region which kept the two nanostructures at a finite distance from each other without physical contact, providing an environment where the negative effect of the Forster energy transfer is diminished. Photocurrent was shown to be a function of broadband visible-light intensity for N–TiO_2 and composite Ag/N–TiO_2 samples. Ag/N–TiO_2 exhibits approximately a linear first-order dependence on the light intensity, while N–TiO_2 exhibits approximately half-order dependence (Fig. 12). The observed linear dependence of the surface concentration of hole on the light intensity for Ag/N–TiO_2 is another indication that charge carriers are formed close to the semiconductor surface in the composite Ag/N–TiO_2 system. Surface-science measurements have implied half-order dependency on light intensity for the TiO_2 bulk holes and linear dependency on light intensity for surface generated holes [171]. In those measurements, the surface-specific formation of charge carriers (holes) was accomplished by using a flux of energetic electrons with penetration depths significantly smaller than those of photons [172]. The observed intensity dependence difference was attributed to the charge carriers formed in the bulk are lost mainly through the process of charge carrier recombination (exhibiting a half-order dependence on the intensity), while the charge carriers formed close to the surface of the semiconductor mainly decayed in their reaction with surface trap states (exhibiting a first-order dependence on the light intensity).

Devi et al., reported the use of Ag/Mn–TiO_2, which showed enhanced photocatalytic activity due to the synergistic effect of bicrystalline framework of anatase and rutile structures with high intimate contact due to the similarity in their crystallite sizes [13c]. The extent of band bending, the variation of potential field in the space charge region with respect to the size of the deposited Ag metal particles was discussed in detail. Metal/semiconductor contact induced band bending due to the variation of electric and potential fields in the space charge region was described by using finite and infinite interface models. The infinite metal/semiconductor interface model can be applied when

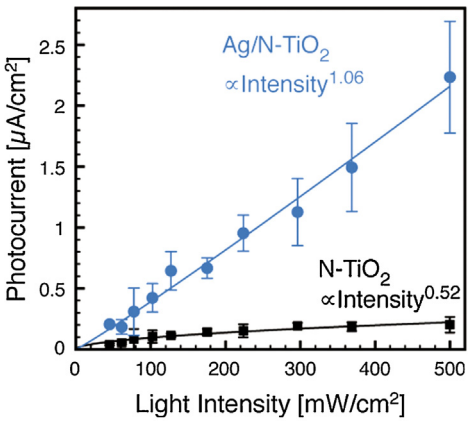

Fig. 12. Photocurrent as a function of broadband visible-light intensity for N–TiO_2 and composite Ag/N–TiO_2 samples Ag/N–TiO_2 exhibits approximately a linear (first-order) dependence on the light intensity, while N–TiO_2 exhibits approximately half-order dependence.
Reprinted with permission from Ref. [169] Copyright (2011) American Chemical Society.

lateral width of metal/semiconductor interface is higher than the thickness of the space charge region (10 nm). However in a catalytic system where semiconductor particles with small metal deposits are used as a catalyst which is smaller than 10 nm, finite metal/semiconductor interface model is more relevant. In this regard Ioannindes and Verykios have proposed a model based on Schottky approximation [20]. According to them the electric field $E(r)$ and potential $V(r)$ in the space charge region along with extent of band bending can be calculated. As the size of Ag metal deposit increases the magnitude of the electric field decreases. It can be inferred that when the radius of the deposited Ag metal particle on the surface of semiconductor is around 8 nm, the number of surface adsorbed molecules is high. The number of adsorbed molecules on the surface decreases with the increase in the size of the metal deposit. Dimensional size of deposited Ag particles plays a significant role in enhancing the photocatalytic activity. Depending on the size of the silver deposit, the energy level of silver varies from −4.64 to −1.30 eV (with respect to vacuum energy level). Beyond the optimum Ag concentration (>0.10%), the space charge region within the semiconductor becomes more negative and facilitates the recombination process. The surface plasmon resonance frequency of the metal particles can be tuned to the visible light absorption by changing the size of the deposited metal particles on the mixed phase titania.

Ag deposited on Fe-doped TiO_2 (Ag/Fe–TiO_2) showed enhanced activity for the photocatalytic degradation of MB under visible light irradiation compared to Ag/TiO_2, Fe/TiO_2 and TiO_2. The superior activity of Ag/Fe–TiO_2 is ascribed to coexistence of optimal Fe^{3+} (0.3 mol%) and Ag (0.25 mol%) content. Under UV illumination electron–hole pairs are generated which are trapped by Fe^{3+} ions hindering recombination process [173]. The trapped electron is further transferred to surface adsorbed oxygen to generate superoxide radical, hydroperoxy and hydroxyl radical. The trapped holes can also generate hydroxyl radical and oxidize the MB molecule. Consequently the Ag nanoparticles can also trap excited electrons and transfer them to adsorbed oxygen to generate superoxide radicals, hydroperoxy and hydroxyl radicals.

$$TiO_2 \xrightarrow{hv} e^- + h^+ \quad (5)$$

$$Fe^{3+} + e^- \rightarrow Fe^{2+} \quad (6)$$

$$Fe^{3+} + h^- \rightarrow Fe^{4+} \quad (7)$$

$$e^- + O_2 \rightarrow O_2^{\bullet -} \quad (8)$$

$$O_2^{\bullet -} + H_2O \rightarrow HOO^{\bullet} + OH^- \quad (9)$$

$$h^+ + H_2O \rightarrow {}^{\bullet}OH + H^+ \quad (10)$$

$${}^{\bullet}OH + \text{Dye} \rightarrow CO_2 + H_2O \quad (11)$$

Under the visible light irradiation, the electronic transition from the dopant energy level (Fe^{3+}/Fe^{4+}) to the CB of TiO_2 is responsible for the excitation of the nanocomposite [174]. The 3d orbital of Fe^{3+} ion is located above the TiO_2VB. Thus Fe^{3+} ion can absorb a photon to produce a Fe^{4+} ion and this excited electron in the TiO_2 CB can either react with the adsorbed oxygen to form superoxide radical or can be subsequently transferred to Ag nanoparticles inhibiting the recombination of electron–hole pairs. In addition, Fe^{4+} ions can react with surface hydroxyl group to produce hydroxyl radical and Fe^{3+} ion (Fig. 13).

$$Fe^{3+} + hv \rightarrow Fe^{4+} + e^- \quad (12)$$

$$e^- + O_2 \rightarrow O_2^{\bullet -} \quad (13)$$

$$Fe^{4+} + OH^- \rightarrow Fe^{3+} + OH^{\bullet} \quad (14)$$

Visible light degradation experiments were conducted in presence of blue, green, yellow and red filters (Table 6) suggested that

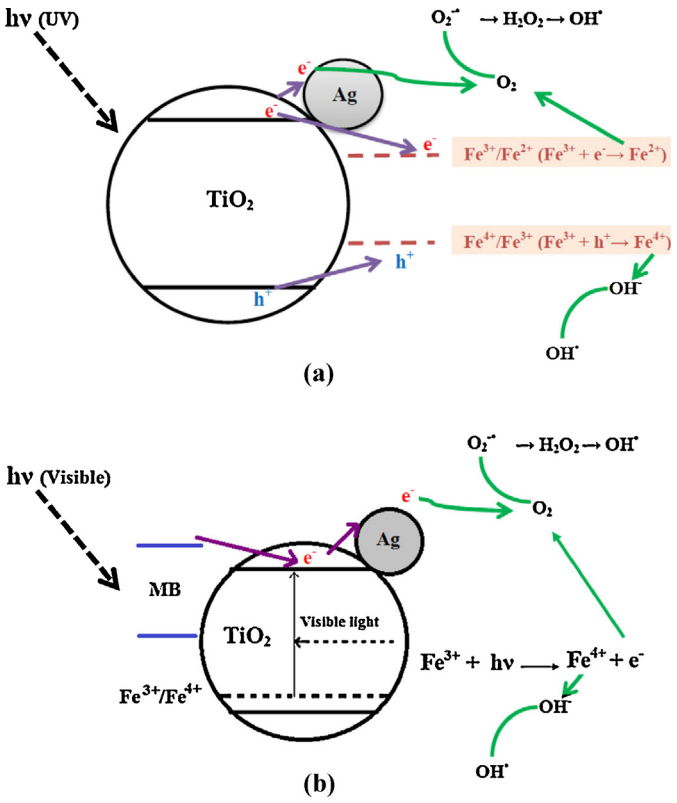

Fig. 13. Schematic diagram of photocatalytic mechanism of Ag/Fe^{3+}–TiO_2 prepared nanocatalyst under (a) UV light and (b) visible light irradiation.
Reprinted with permission from Ref. [173] Copyright (2014) Elsevier.

red filter transmits most of visible light at $\lambda > 600$ nm where MB is activated into its excited state injecting an electron into the CB or surface states of TiO_2 which was captured by surface adsorbed oxygen to generate superoxide radical [175]. In another study Fe^{3+} ions were doped into TiO_2 nanotube arrays synthesized by electrochemical anodic oxidation of pure titanium in an NH_4F electrolyte solution containing iron ions. Ag nanoparticles were assembled on this Fe^{3+}–TiO_2 nanotube array by microwave assisted chemical reduction method which showed enhanced quantum efficiency for H_2 production by water splitting under UV/visible light irradiation [176]. Both Ag and Fe effectively restrained the recombination rate of photogenerated charge carriers. During H_2 production ethanol is oxidized to acetic acid by hydroxyl radicals. The consumption of hydroxyl radicals accelerates the decomposition of water to H^+ and hydroxyl radicals. When UV light is irradiated on Ag/Fe^{3+}–TiO_2 electron gets excited from VB to Fe^{3+} dopant level to yield Fe^{2+} leaving behind a hole. This Fe^{2+} in turn is reoxidized to Fe^{3+} by transfer of electron to adsorbed oxygen. Alternatively the trapped hole can migrate to Fe^{3+} dopant to yield Fe^{4+} which in turn can transfer the hole to the surface and oxidize the hydroxyl anions to produce hydroxyl radicals. Fe^{3+} ion is relatively stable ion state due to half filled 3d electronic configuration. The Fe^{4+} or Fe^{2+} states can easily release the respective charge carriers to return back to stable Fe^{3+} state and thereby participating in the photocatalytic reaction [177,178]. Ag/Fe–TiO_2 (with 4.5% Fe and Ag) showed enhanced photocatalytic hydrogen production via water splitting under visible light irradiation [179]. During the hydrogen production, ethanol is used as sacrificial agent. Holes in TiO_2 VB react with water to form an H^+ ion and a hydroxyl free radical ($OH^{\bullet}$). Subsequently hydroxyl free radicals can participate in the chemical reaction with CH_3CH_2OH [180]. The decomposition of water to H^+ and hydroxyl

Table 6
The percentage of MB discoloration and TOC reduction by different catalyst under visible light in presence of various filters.

Samples	% Discoloration						K (h^{-1})	% TOC reduction	
	Visible light		Filters				Visible light	Visible light	
	240 min irradiation	540 min irradiation	Blue filter	Green filter	Yellow filter	Red filter	240 min irradiation	240 min irradiation	540 min irradiation
TiO_2	22.0	64.0	6.0	6.0	12.7	10.0	0.054	5	16
Fe^{3+}–TiO_2	43.0	86.0	17.0	14.8	22.9	12.7	0.138	10	36
Ag/TiO_2	37.0	75.0	18.0	11.4	16.3	15.0	0.102	8	30
Ag/Fe^{3+}–TiO_2	52.0	99.0	25.0	24.0	23.6	24.0	0.180	12	47

Reprinted with permission from Ref. [173] Copyright (2014) Elsevier.

radicals is accelerated by the presence of sacrificial agent leading to enhanced hydrogen production [181].

TiO_2 encapsulated Ag nanoparticles supported on porous SiO_2 bead nanospheres were fabricated in the following way: surface protected etching strategy was adopted to synthesize porous SiO_2 core, followed by a calcination process to immobilize Ag nanoparticles on the surface of porous SiO_2 and in turn this was followed by hydrolysis process to coat TiO_2 shell layer, respectively [182]. This photocatalyst showed enhanced photocatalytic activity for RhB degradation when compared to TiO_2 encapsulated porous SiO_2 nanospheres and P25 mainly because Ag nanoparticles cannot only enhance the response of UV/visible light while the special structure of TiO_2 encapsulated Ag nanoparticles supported on porous SiO_2 bead nanospheres effectively facilitates the separation of photogenerated electrons and holes. This unique structure of the photocatalyst provides more advantages like: (i) the encapsulation of Ag nanoparticles was advantageous since this process increased its stability during calcination and subsequent photocatalysis. Further, encapsulation effectively avoids the Ag nanoparticles from moving together and coagulating [183–185]. (ii) The in situ growth of the Ag nanoparticles on the surface of porous silica bead leads to uniform distribution of the Ag nanoparticles inside the TiO_2 matrix. This is beneficial to decrease the mean free path of the photogenerated electrons between TiO_2 and Ag nanoparticles which serve as electron trapping center. Furthermore, the authors claim that due to SPR effect of the Ag nanoparticles, the absorption ability of the photocatalyst was largely increased especially in the visible light region [186]. (iii) The encapsulation of Ag within TiO_2 shell increases the contact area between Ag nanoparticles and the TiO_2 matrix for more efficient electron transfer [147]. In another study TiO_2 film was initially prepared by absorptive self assembly method and Ag deposition was fabricated by photochemical route and this Ag/TiO_2/SiO_2 photocatalyst showed improved *E. coli* bactericidal efficiency under UV light illumination [187]. At the intimate contact interface, the plasma Ag metal served as the electron conductors to transport them away from TiO_2 surface and retard the electron–hole recombination rate [188]. The residual free holes can react with water molecules to generate various reactive oxygen species which acts as an immense oxidizing agent and this was the main mechanism proposed for Ag/TiO_2/SiO_2 composite catalyst to kill the bacteria by the assistance of light [189]. Ag/AgCl/TiO_2 nanotube arrays was prepared by depositing AgCl nanoparticles into the self-organized TiO_2 and then partially reducing Ag^+ ions to Ag^0 species on the surface region of AgCl particles under xenon lamp irradiation [190]. The prepared metal–semiconductor nanocomposite plasmonic photocatalyst exhibits high visible-light photocatalytic activity for the degradation of MO in water. The Ag nanoparticles are photoexcited due to SPR effect and charge separation is accomplished by the transfer of photoexcited electrons from the Ag nanoparticles to the TiO_2 CB and the authors further propose simultaneous transfer of compensative electrons from donor Cl^- ions to the Ag nanoparticles (Fig. 14) [191–193]. In another study Ag/AgCl/TiO_2 nanocomposite thin films prepared by the same method exhibited enhanced photocatalytic decomposition of 4-CP under visible light irradiation [194]. The grains of AgCl are photosensitive to UV light due to the ionic point defects and they can trap electron which leads to the formation of small amount of metallic Ag which gets deposited on the surface of AgCl [195]. Under the visible light irradiation electron–hole pairs are photogenerated in the Ag nanoparticles due to SPR effect. The photoexcited electrons of Ag get injected into the TiO_2 CB as the Fermi level of TiO_2 and Ag nanoparticles match with each other thereby forming $Ag^{\bullet+}$. This radical ion can react with Cl^- ion forming Cl^0 and Ag as shown in the equations [191–193]. Because of the high oxidation ability of the chlorine atoms, the 4-CP could be oxidized by the chlorine atoms and hence the Cl^0 could be reduced to chloride ions again. The 4-CP can also be oxidized directly by plasmon induced hole (or Ag^+) on Ag nanoparticles, thereby accelerating the reduction of photooxidized Ag nanoparticles back to their initial state. Therefore, the Ag nanoparticles can be rapidly regenerated and the Ag/AgCl/TiO_2 system remains self stable [196].

$$Ag + hv \rightarrow Ag^* \quad (15)$$

$$Ag^* + TiO_2 \rightarrow Ag^{\bullet+} + TiO_2(e^-) \quad (16)$$

$$TiO_2(e^-) + O_2 \rightarrow TiO_2 + O_2^{\bullet-} \quad (17)$$

$$O_2^{\bullet-} + H^+ \rightarrow HOO^{\bullet} \quad (18)$$

$$e^- + HOO^{\bullet} + H^+ \rightarrow H_2O_2 \quad (19)$$

$$H_2O_2 + e^- \rightarrow {}^{\bullet}OH + OH^- \quad (20)$$

$$4\text{-CP} + {}^{\bullet}OH \rightarrow CO_2 + H_2O + Cl^- \quad (21)$$

$$Ag^{\bullet+} + Cl^- \rightarrow Ag + Cl^0 \quad (22)$$

$$4\text{-CP} + Cl^0(h^+) \rightarrow CO_2 + H_2O + Cl^- \quad (23)$$

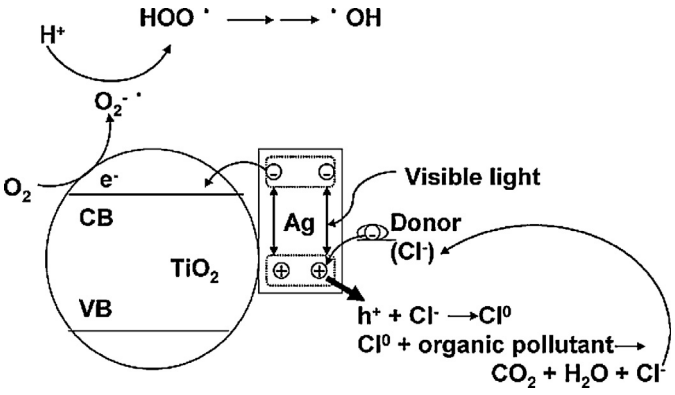

Fig. 14. Schematic representation for the charge separation in a visible light irradiated Ag/AgCl/TiO_2 system.

Reprinted with permission from Ref. [190] Copyright (2009) American Chemical Society.

Considering their large specific surface area, high pore volume, unique morphology and high photocatalytic activity, these photocatalysts are of great interest in various applications like sensors, solar cell, catalysis, separation technology, biomedical engineering and nanotechnology. This study may provide new insight into the design and preparation of advanced visible-light photocatalytic materials.

5. Photocatalytic activity of palladium deposited titania (Pd/TiO_2)

Bowker and co-workers studied the photocatalytic degradation of methanol on a Pd/TiO_2 catalyst under anaerobic conditions, which clearly indicated that the active sites were on the metal/TiO_2 interface [197]. The high photoactivity of Pd/N–TiO_2 (0.6% Pd) for eosin yellow decomposition under visible light arises from the synergistic effects of palladium deposition and nitrogen doping [198]. The palladium on TiO_2 surface creates a Schottky junction between the metal and the semiconductor, which acts as a sink for photogenerated electrons. Plasmonic cubic Pd@TiO_2 composite structure with well-controlled TiO_2 shell thickness of 75 nm fabricated using a two-step surface modification process exhibited superior visible light photocatalytic performance for phenol degradation. The superior activity was contributed to the synergistic effects between large surface area with high crystallinity and well defined morphology with controllable optical properties from plasmonic effects [199]. The Pd core serves as a sensitizer that absorbs resonance photons, facilitates light harvest by enhancing light absorption. During this process collective oscillation of valence electrons of the metal on interaction with incident light excites electrons from the ground state to the SPR state which has energy between 1.0 and 4.0 eV with respect to Fermi level of the Pd metal [200]. These photoexcited electrons directly get injected into the nearby TiO_2 CB due to the formation of Schottky barrier at the metal semiconductor interface. It was also suggested that the hot spots (plasmon decay producing intensely hot electrons) appear on the sharp edges and corners of TiO_2 where the electric field intensity of SPR is several times higher than that of the incident electric field of the photon [201–204]. Electron hole pairs are generated by surface plasmon decay and the rate of generation is intensified by the local filed enhancement on the hot spot regions (Fig. 15). This system may pave way for utilizing the SPR effect in designing highly efficient photocatalytic system. In another research study it was found that Pd/TiO_2 (containing 0–44% rutile) had significant number of Ti^{3+} sites which was in contact with Pd and was responsible for ethylene selectivity in acetylene hydrogenation reaction [205]. The existence of highly distorted defect sites at the metal–semiconductor interfaces are the source of efficient and unique photocatalytic reaction sites [205].

6. Photocatalytic activity of titania with bimetallic surface deposition

Recent literature highlights various research groups investigating the effects of bimetallic deposition on TiO_2 surface. However this review gives only a glimpse toward this strategy. Detailed analogy and citations of all the articles of this aspect is too difficult at this stage and it may be a subject matter for another complete review. Bimetallic particles of same size, shape, and composition show significant differences in activity when configured into different architectures such as alloy, cluster in cluster, core–shell or monometallic mixtures. The structure of bimetallic combination depends on the preparation conditions, miscibility and the kinetics of the reduction of metal ions on the surface of the catalyst [206–210]. Au/Pt–TiO_2 obtained by the hydrolysis of titanium isopropoxide in microemulsion system followed by reduction of $HAuCl_4$ (precursor for gold) and K_2PtCl_4 (precursor for palladium) along with $NaBH_4$ for the bimetallic deposition and the catalyst was further calcined at 450 °C. This catalyst exhibited high rates for phenol degradation under visible light irradiation [210]. The use of $NaBH_4$ as reducing agent favored the formation of smaller Au/Pt nanoparticles and higher amounts of gold in the form of electronegative species ($Au^{\delta-}$) and the intermetallic dominant state (AuPt) facilitates the charge transfer mechanism between the metals. The electron transport is expected to take place from Pt to Au due to the higher electronegative potential of gold compared to Pt. It was also observed that enhancement in the calcination temperature of this photocatalyst from 450 to 650 °C (Table 7) resulted in rapid drop of photoactivity due to the shrinkage in the surface area, change in the crystal structure and probably change in AuPt nanoparticle morphology [210]. Au/Pt/TiO_2 electrospun nanofibers showed direct evidence for Plasmon enhanced H_2 generation through dual-beam irradiation [211]. The Au/Pt/TiO_2 nanofibers exhibited certain activity for H_2 under single irradiation at 420 nm that excites the defect/impurity states of TiO_2. A higher activity (2.5 times) for H_2 generation was observed when secondary irradiation at 550 nm which was introduced simultaneously to excite Au SPR.

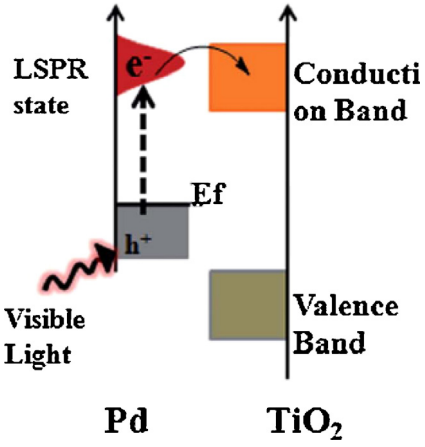

Fig. 15. Hot electron injection from the surface plasmon state of the metal to the CB of TiO_2 in Pd/TiO_2 composite.
Reprinted with permission from Ref. [199] Copyright (2014) Royal Society of Chemistry.

Table 7
Surface area and photoactivity of TiO_2 modified with Au/Pt obtained by microemulsion method by using titanium isopropoxide as TiO_2 source and $NaBH_4$ as reducing agent.

Sample label	Amount of noble metal precursor (mol%)		Calcination temperature (°C)	BET surface area (m^2/g)	Rate of phenol degradation under visible light ($\lambda > 420$ nm) $\mu mol\ dm^{-3}\ min^{-1}$
	Pt	Au			
(0.5)Au/(0.1)Pt/TiO_2-350	0.1	0.5	350	195	0.42
(0.5)Au/(0.1)Pt/TiO_2-450	0.1	0.5	450	160	1.71
(0.5)Au/(0.1)Pt/TiO_2-550	0.1	0.5	550	128	0.69
(0.5)Au/(0.1)Pt/TiO_2-650	0.1	0.5	650	98	0.27

Reprinted with permission from Ref. [210] Copyright (2014) Elsevier.

The control experiments with different sacrificial agents like isopropanol, triethanolamine (TEOA), and methanol suggested that the hot plasmonic electrons of Au are responsible for the enhanced photocatalytic activity. An enhancement was observed in the case of TEOA and isopropanol but no such effect of enhancement was observed with methanol. This different enhancement factor suggests that the strong localized electric field by SPR excitation may not be the dominating factor on the enhanced H_2 generation [211].

The electrospun TiO_2 nanofibers decorated with Au 0.75 at%/Pd 0.25 at% bimetallic alloy nanoparticles displayed a high selectivity for H_2 production rate (88.5 μmol h^{-1}) through decomposition of formic acid due to the high selectivity of Pd for the dehydrogenation reaction, the strong electron sink effect of Au/Pd nanoparticles and the SPR effect of Au [212].

Ag/Pt/TiO_2 bimetallic modified TiO_2 nanoparticles exhibited improved photocatalytic activity for the degradation of phenol under visible light irradiation compared to monometallic Ag/TiO_2 and Pt/TiO_2 nanoparticles [213]. Antimicrobial activities were only observed for Ag/TiO_2 and Ag/Pt/TiO_2 photocatalysts for inactivation of bacteria like *E. coli* and *S. aureus*.

7. Conclusion

A comprehensive update of mechanism and kinetics involved behind the enhanced photocatalytic efficiency of TiO_2 in combination with the deposited noble metals like Pt, Au, Ag and Pd is discussed elaborately and an effort is made to give an insight involving various strategies adopted along with the highlights and advancements made in the research field. Several milestones in tailoring the interface and bulk properties between TiO_2 and the metal are explored. Though it is impossible to cover all the research articles due to the voluminous work available in the literature, we sincerely hope that this particular review will trigger interest in synthesizing several semiconductors with multi functional features to enhance its capacity in the energy and environment applications. The degree of enhancement of TiO_2 activity by metallization seems to be highly depending on several factors like the substrate to be degraded, the effects of metal/TiO_2 interactions, the amount and the nature of deposited metal, structural and morphological properties of original TiO_2, photophysical and photochemical properties, site specific interaction, electrostatic effects, surface adsorption, metallic nature and size of the deposits, oxidation state of the metal which influences the redox properties of the photocatalyst are discussed elaborately in the present review.

The efficiency of the metalized semiconductor particles in photocatalysis and photoelectrocatalysis is dictated by the factors like variation of electric field and potential field within the space charge region and also on the extent of band bending. Electric filed decreases with increase in the size of the metal deposit whereas the potential field shows an exponential behavior with the increase in size of the metal deposits. Majority of studies report the optimum size of the metal to be between 8 and 12 nm and the maximum efficiency of the catalyst is limited to this size. The process of oxidation of deposited metal by the photogenerated hole and the process of reduction of metal ions by CB electrons compete with one another to decide the ultimate fate of the interface. The challenge for the next decade lies in designing a novel metal semiconductor assembly which can promote an efficient photoinduced charge separation and which can mimic various reactions taking place in the nature. The other applications of metallized semiconductor particles include as colorimetric sensor, photovoltaic and also in photochromic devices. It is hoped that this review can inspire multidisciplinary research interest in precisely tailoring the photophysical and photochemical properties of metal deposited semiconductor particles and to study in the realm of various applications.

Acknowledgements

The authors acknowledge University Grants Commission (UGC) and Department of Science and Technology (DST-IDP & DST-SERC), Government of India for their financial supports.

References

[1] P.V. Kamat, J. Phys. Chem. B 106 (106) (2002) 7729–7744.
[2] S.K. Dutta, S.K. Mehetor, N. Pradhan, J. Phys. Chem. Lett. 3 (2015) 936–944.
[3] A.L. Linsebigler, G. Lu, J.T. Yates, Chem. Rev. 95 (1995) 735–758.
[4] X. Chen, A. Selloni, Chem. Rev. 114 (2014) 9281–9282.
[5] M. Dahl, Y. Liu, Y. Yin, Chem. Rev. 114 (2014) 9853–9889.
[6] J. Bai, B. Zhou, Chem. Rev. 114 (2014) 10131–10176.
[7] G. Liu, H.G. Yang, J. Pan, Y.Q. Yanh, G.Q.M. Lu, H.M. Cheng, Chem. Rev. 114 (2014) 9559–9612.
[8] K. Bourikas, C. Kordulis, A. Lycourghiotis, Chem. Rev. 114 (2014) 9754–9823.
[9] (a) S.G. Kumar, L.G. Devi, J. Phys. Chem. A 115 (2011) 13211–13241; (b) L.G. Devi, S.G. Kumar, Cent. Eur. J. Chem. 3 (2011) 959–961.
[10] (a) L.G. Devi, R. Kavitha, Appl. Catal. B: Environ. 140–141 (2013) 559–587; (b) L.G. Devi, R. Kavitha, RSC Adv. 4 (2014) 28265–28299.
[11] (a) L.G. Devi, R. Kavitha, Mater. Chem. Phys. 143 (2014) 1300–1308; (b) R. Kavitha, L.G. Devi, J. Environ. Chem. Eng. 2 (2014) 857–867; (c) L.G. Devi, R. Kavitha, B. Nagaraj, Mater. Sci. Semicond. Process 40 (2015) 832–839.
[12] (a) L.G. Devi, N. Kottam, S.G. Kumar, J. Phys. Chem. C 113 (2009) 15593–15601; (b) L.G. Devi, N. Kottam, S.G. Kumar, K.S.A. Raju, Catal. Lett. 131 (2009) 612–617; (c) L.G. Devi, S.G. Kumar, B.N. Murthy, N. Kottam, Catal. Commun. 10 (2009) 794–798; (d) L.G. Devi, N. Kottam, B.N. Murthy, S.G. Kumar, J. Mol. Catal. A: Chem. 328 (2010) 44–52; (e) L.G. Devi, N. Kottam, S.G. Kumar, K.E. Rajashekhar, Cent. Eur. J. Chem. 8 (2010) 142–148; (f) L.G. Devi, S.G. Kumar, Appl. Surf. Sci. 257 (2011) 2779–2790.
[13] (a) L.G. Devi, B. Nagaraj, Photochem. Photobiol. 90 (2014) 1089–1098; (b) L.G. Devi, B. Nagaraj, K.E. Rajashekhar, Chem. Eng. J. 181–182 (2012) 259–266; (c) B. Nagaraj, L.G. Devi, J. Mol. Catal. A: Chem. 390 (2014) 142–151.
[14] (a) F. Dong, Q. Li, Y. Sun, W.K. Ho, ACS Catal. 4 (2014) 4341–4350; (b) F. Dong, Q. Li, Y. Zhou, Y. Sun, H. Zhang, Z. Wu, Dalton Trans. 43 (2014) 9468–9480.
[15] (a) F. Dong, H. Wang, G. Sen, Z. Wu, S.C. Lee, J. Hazard. Mater. 187 (2011) 509–516; (b) F. Dong, T. Xiong, Y. Sun, Z. Zhao, Y. Zhou, X. Feng, Z. Wu, Chem. Commun. 50 (2014) 10386–10389.
[16] H. Geriscber, A. Heller, J. Phys. Chem. 95 (1991) 5261–5267.
[17] P.V. Kamat, J. Phys. Chem. C 111 (2007) 2834–2860.
[18] M. Jakob, H. Levanon, P.V. Kamat, Nano Lett. 3 (2003) 353–358.
[19] S.K. Ghosh, T. Pal, Chem. Rev. 107 (2007) 4797–4862.
[20] (a) Z. Zhang, J.T. Yates Jr., Chem. Rev. 112 (2012) 5520–5551; (b) T. Ioannides, X.E. Verykios, J. Catal. 161 (1996) 560–569.
[21] M.L. Brongersma, N.J. Halas, P. Nordlandu, Nat. Nanotechnol. 10 (2015) 25–34.
[22] E. Hutter, J.H. Fendler, Adv. Mater. 16 (2004) 1658–1706.
[23] S. Link, M.A. El-Sayed, J. Phys. Chem. B 103 (1999) 4212–4217.
[24] (a) M. Rycenga, M.R. Langille, M.L. Personick, T. Ozel, C.A. Mirkin, Nano Lett. 12 (2012) 6218–6222; (b) X. Ji, X. Song, J. li, Y. Bai, W. Yang, X. Peng, J. Am. Chem. Soc. 129 (2007) 13939–13948; (c) F. Möllers, H.J. Tolle, R. Memming, J. Electrochem. Soc. 121 (1974) 1160–1167; (d) M. Rycenga, C.M. Cobley, J. Zeng, W. Li, C.H. Moran, Q. Zhang, D. Qin, Y. Xia, Chem. Rev. 111 (2011) 3669–3712; (e) S. Bonanni, K. Aït-Mansour, W. Harbich, H. Brune, J. Am. Chem. Soc. 134 (2012) 3445–3450.
[25] (a) P.H.C. Camargo, C.M. Cobley, M. Rycenga, Y. Xia, Nanotechnology 20 (2009) 434020; (b) F. Tam, G.P. Goodrich, B.R. Johnson, N.J. Halas, Nano Lett. 7 (2007) 496–501.
[26] H. Gerisher, eds. D.F. Ollis, H. AlEkabi (Elsevier Science Publishers B. V., 1, 1993).
[27] T. Sakata, T. Kawai, K. Hashimoto, Chem. Phys. Lett. 88 (1982) 50–54.
[28] J. Disdier, J.M. Herrmann, P. Pichat, J. Chem. Soc. Faraday Trans. 79 (1983) 651–660.
[29] P.V. Kamat, Pure Appl. Chem. 74 (2002) 1693–1706.
[30] (a) A. Wood, M. Giersig, P. Mulvaney, J. Phys. Chem. B 105 (2001) 8810–8815;

(b) Y. Nakato, K. Ueda, H. Yano, H. Tsubomura, J. Phys. Chem. 92 (1988) 2316–2324.
[31] T. Ioannides, X.E. Verykios, J. Catal. 161 (1996) 560–569.
[32] M. Pujadas, P. Salvador, J. Electrochem. Soc. 136 (1989) 716–723.
[33] T. Torimoto, S. Nakamura, S. Ikeda, B. Ohtani, Phys. Chem. Chem. Phys. 4 (2002) 5910–5914.
[34] M. Moonsiri, P. Rangsunvigit, S. Chavadej, E. Gulari, Chem. Eng. J. 97 (2004) 241–248.
[35] F. Bosc, A. Ayral, N. Keller, V. Keller, Appl. Catal. B: Environ. 69 (2007) 133–137.
[36] F. Bosc, A. Ayral, P. Albouy, C. Guizard, Chem. Mater. 15 (2003) 2463–2468.
[37] M.C. Hidalgo, M. Maicu, J.A. Navio, G. Colon, Catal. Today 129 (2007) 43–49.
[38] S. Sakthivel, M.V. Shankar, M. Palanichamy, B. Arabindoo, D.W. Bahnemann, V. Murugesan, Water Res. 38 (2004) 3001–3008.
[39] F.B. Li, X.Z. Li, Chemosphere 48 (2002) 1103–1111.
[40] (a) J.C. Yang, Y.C. Kim, Y.G. Shul, C.H. Shin, T.K. Lee, Appl. Surf. Sci. 121–122 (1997) 525–529;
(b) A.V. Vorontsov, E.N. Savinov, Z.S. Jin, J. Photochem. Photobiol. A: Chem. 125 (1999) 113–117.
[41] C. Wang, R. Pagel, J.K. Dohrmann, D.W. Bahnemann, C. R. Chim. 9 (2006) 761–773.
[42] H. Park, J. Lee, W. Choi, Catal. Today 111 (2006) 259–265.
[43] H. Park, W. Choi, J. Phys. Chem. B 107 (2003) 3885–3890.
[44] M.R. Hoffmann, S.T. Martin, W. Choi, D.W. Bahnemann, Chem. Rev. 95 (1995) 69–96.
[45] W. Choi, A. Termin, M.R. Hoffmann, J. Phys. Chem. 98 (1994) 13669–13679.
[46] (a) C. Millon, D. Riassetto, G. Berthome, F. Roussel, M. Langlet, J. Photochem. Photobiol. A: Chem. 189 (2007) 334–348;
(b) J. Wang, P. Yang, B. Cao, J. Zhao, Z. Zhu, Appl. Surf. Sci. 325 (2015) 86–90.
[47] A. Yee, S.J. Morrison, H. Idriss, J. Catal. 191 (2000) 30–45.
[48] M. Maicu, M.C. Hidalgo, G. Colon, J.A. Navio, J. Photochem. Photobiol. A: Chem. 217 (2011) 275–283.
[49] (a) A. Roucoux, J. Schlz, H. Patin, Chem. Rev. 102 (2002) 3757–3778;
(b) N.R. Jana, T.K. Sau, T. Pal, J. Phys. Chem. B 103 (1999) 115–121.
[50] D.V. Kozlov, A.V. Vorontsov, J. Catal. 258 (2008) 87–94.
[51] (a) J. Lee, W. Choi, J. Phys. Chem. B 109 (2005) 7399–7406;
(b) S. Kim, W. Choi, J. Phys. Chem. B 106 (2002) 13311–13317.
[52] A. Linsebigler, C. Rusu, J.T. Yates Jr., J. Am. Chem. Soc. 118 (1996) 5284–5289.
[53] M.D. Driessen, V.H. Grassian, J. Phys. Chem. B 102 (1998) 1418–1423.
[54] J. Fan, J.T. Yates Jr., J. Am. Chem. Soc. 118 (1996) 4686–4692.
[55] E.A. Kozlova, T.P. Lyubina, M.A. Nasalevich, A.V. Vorontsov, A.V. Miller, V.V. Kaichev, V.N. Parmon, Catal. Commun. 12 (2011) 597–601.
[56] C. Wang, L. Yin, L. Zhang, N. Liu, N. Lun, Y. Qi, ACS Appl. Mater. Interfaces 2 (2010) 3373–3377.
[57] H.B. Zeng, W.P. Cai, P.S. Liu, X.X. Xu, H.J. Zhou, C. Klingshirn, H. Kalt, ACS Nano 2 (2008) 1661–1670.
[58] W. Mu, J.M. Herrmann, P. Pichat, Catal. Lett. 3 (1989) 73–84.
[59] A.V. Rosario, E.C. Pereira, Appl. Catal. B: Environ. 144 (2014) 840–845.
[60] (a) K.M. Schindler, M. Kunst, J. Phys. Chem. 94 (1990) 8222–8226;
(b) D.C. Hurum, A.G. Agrios, K.A. Gray, T. Rajh, M.C. Thurnauer, J. Phys. Chem. B 107 (2003) 4545–4549.
[61] S.N. Basahel, K. Lee, R. Hahn, P. Schmuki, S.M. Bawaked, S.A.A. Thabaiti, Chem. Commun. 50 (2014) 6123–6125.
[62] S. Yin, T. Sato, J. Photochem. Photobiol. A: Chem. 169 (2005) 89–94.
[63] B. Wang, Z. Yang, H. An, J. Zhai, Q. Li, H. Cui, Appl. Surf. Sci. 324 (2015) 817–824.
[64] M. Karkmaz, C. Puzenat, C. Guillard, J.M. Herrmann, Appl. Catal. B: Environ. 51 (2004) 183–194.
[65] (a) P. Konarski, A. Zawada, S. Kowalczyk, K.J. Rezler, Surf. Interface Anal. 45 (2013) 592–595;
(b) P. Huo, Z. Lu, H. Wang, J. Pan, H. Li, X. Wu, W. Huang, Y. Yan, Chem. Eng. J. 172 (2011) 615–622.
[66] C.C. Justin, M. Kunst, D. Huguenin, J. Mater. Sci. 38 (2003) 2429–2437.
[67] J. Chen, D.F. Ollis, W.H. Rulkens, H. Bruning, Water Res. 33 (1999) 661–668.
[68] (a) A.A. Ismail, D.W. Bahnemann, Green Chem. 13 (2011) 428–435;
(b) L. Qi, W. Ho, J. Wang, P. Zhang, J. Yu, Catal. Sci. Technol. 5 (2015) 2366–2377.
[69] (a) N. Lakshminarasimhan, E. Bae, W. Choi, J. Phys. Chem. C 111 (2007) 15244–15250;
(b) Y. Huang, W. Ho, S. Lee, L. Zhang, G. Li, J.C. Yu, Langmuir 24 (2008) 3510–3516.
[70] (a) C. Wang, R. Pagel, J.K. Dohemann, D.W. Bahnemann, Mater. Sci. Forum 544–545 (2007) 17–22;
(b) C.Y. Wang, D.W. Bahnemann, J.K. Dohrmann, Chem. Commun. (2000) 1539–1540;
(c) C.Y. Wang, C. Bottcher, D.W. Bahnemann, J.K. Dohrmann, J. Mater. Chem. 13 (2003) 2322–2329.
[71] J. Yu, L. Qi, M. Jaroniec, J. Phys. Chem. C 114 (2010) 13118–13125.
[72] (a) G.A. Hope, A.J. Bard, Phys. Chem. 87 (1983) 1979–1984;
(b) K.E. Karakitsou, X.E. Verykios, J. Phys. Chem. 97 (1993) 1184–1189.
[73] (a) J. Mao, L. Ye, K. Li, X. Zhang, J. Liu, T. Peng, L. Zan, Appl. Catal. B: Environ. 144 (2014) 855–862;
(b) J. Yu, J. Low, W. Xiao, P. Zhou, M. Jaroniec, J. Am. Chem. Soc. 136 (2014) 8839–8842.
[74] W.N. Wang, W.J. An, B. Ramalingam, S. Mukherjee, D.M. Niedzwiedzki, S. Gangopadhyay, P. Biswas, J. Am. Chem. Soc. 134 (2012) 11276–11281.
[75] S.C. Chan, M.A. Barteau, Langmuir 21 (2005) 5588–5595.
[76] J. Zhang, L. Li, T. Yan, G. Li, J. Phys. Chem. C 115 (2011) 13820–13828.
[77] V. Celik, H. Unal, E. Mete, S. Ellialtioglu, Phys. Rev. B 82 (2010) 205113.
[78] (a) C.W. Oatley, Phys. Soc. Lond. 51 (1939) 318;
(b) A. Imanishi, E. Tsuji, Y. Nakato, J. Phys. Chem. C 111 (2007) 2128–2132.
[79] (a) L. Qi, J. Yu, M. Jaroniec, Phys. Chem. Chem. Phys. 13 (2011) 8915–8923;
(b) L. Nie, P. Zhou, J. Yu, M. Jaroniec, J. Mol. Catal. A: Chem. 390 (2014) 7–13.
[80] J. Yu, L. Yue, S.W. Liu, B.B. Huang, X.Y. Zhang, J. Colloid Interface Sci. 334 (2009) 58–64.
[81] (a) J. Yu, J.F. Xiong, B. Cheng, S.W. Liu, Appl. Catal. B: Environ. 60 (2005) 211–221;
(b) B. Cheng, Y. Le, J. Yu, J. Hazard. Mater. 177 (2010) 971–977.
[82] (a) J. Yu, W.G. Wang, B. Cheng, B.L. Su, J. Phys. Chem. C 113 (2009) 6743–6750;
(b) Q.J. Xiang, K.L. Lv, J. Yu, Appl. Catal. B: Environ. 96 (2010) 557–564.
[83] J.Y. Park, G.A. Somorjai, Chem. Phys. Chem. 7 (2006) 1409–1413.
[84] B. Sun, A.V. Vorontsov, P.G. Smirniotis, Langmuir 19 (2003) 3151–3156.
[85] (a) B. Ohtani, K. Iwai, S.I. Nishimoto, S. Sato, J. Phys. Chem. B 101 (1997) 3349–3359;
(b) S. Nishimoto, B. Ohtani, T. Kagiya, J. Chem. Soc. Faraday Trans. 81 (1985) 2467–2474.
[86] (a) A. Pandikumar, S. Murugesan, R. Ramaraj, ACS Appl. Catal. Sci. Interfaces 2 (2010) 1912–1917;
(b) A. Pandikumar, S. Manonmani, R. Ramaraj, Catal. Sci. Technol. 2 (2012) 345–353;
(c) A. Pandikumar, K. Sivaranjani, C.S. Gopinath, R. Ramaraj, RSC Adv. 3 (2013) 13390–13398;
(d) S. Jayabal, A. Pandikumar, H. Ngee Lim, R. Ramaraj, T. Sund, N.M. Huang, Analyst 140 (2015) 2540–2555;
(e) J. Ma, S. Guo, X. Guo, H. Ge, Appl. Surf. Sci. 353 (2015) 1117–1125.
[87] (a) M.C. Hidalgo, M. Maicu, J.A. Navio, G. Colon, Appl. Catal. B: Environ. 81 (2008) 49–55;
(b) M.C. Hidalgo, M. Maicu, J.A. Navio, G. Colon, J. Phys. Chem. C 113 (2003) 12840–12847;
(c) Z. Xu, J. Yu, G. Liu, Electrochem. Commun. 13 (2011) 1260–1263;
(d) J. Fang, S.W. Cao, Z. Wang, M.M. Shahjamali, S.C.J. Loo, J. Barber, C. Xue, Int. J. Hydrogen Energy 37 (2012) 17853–17861;
(e) D. Zhao, Y. Yu, H. Long, Y. Cao, Appl. Surf. Sci. 315 (2014) 247–251.
[88] P. Mohapatra, J. Moma, K.M. Parida, W.A. Jordaan, M.S. Scurrell, Chem. Commun. (2007) 1044–1046.
[89] V. Subramanian, E.E. Wolf, P.V. Kamat, J. Am. Chem. Soc. 126 (2004) 4943–4950.
[90] E. Kowalska, R. Abea, B. Ohtani, Chem. Commun. 2 (2009) 241–243.
[91] Y. Tian, T. Tatsuma, J. Am. Chem. Soc. 127 (2005) 7632–7637.
[92] V. Subramanian, E. Wolf, P.V. Kamat, Langmuir 19 (2003) 469–474.
[93] A.V. Rupa, D. Divakar, T. Siva Kumar, Catal. Lett. 132 (2009) 259–267.
[94] K. Okazaki, Y. Morikawa, S. Tanaka, K. Tanaka, M. Kohyama, Phys. Rev. B 69 (2004) 235404.
[95] B. Tian, J. Zhang, T. Tong, F. Chen, Appl. Catal. B: Environ. 79 (2008) 394–401.
[96] M. Sadeghi, W. Liu, T.G. Zhang, P. Stavropoulos, B. Levy, J. Phys. Chem. 100 (1996) 19466–19474.
[97] M.C. Hidalgo, J.J. Murcia, J.A. Navío, G. Colon, Appl. Catal. A: Gen. 397 (2011) 112–120.
[98] Z. Pei, L. Ding, W. Feng, S. Weng, P. Liu, Phys. Chem. Chem. Phys. 16 (2014) 21876–21881.
[99] (a) F. Zuo, L. Wang, T. Wu, Z. Zhang, D. Borchardt, P. Feng, J. Am. Chem. Soc. 132 (2010) 11856–11857;
(b) X. Pan, Y. Xu, Appl. Catal. A: Gen. 459 (2013) 34–40.
[100] A. Kogo, N. Sakai, T. Tatsuma, Electrochem. Commun. 12 (2010) 996–999.
[101] W. Hou, Z. Liu, P. Pavaskar, W.H. Hung, S.B. Cronin, J. Catal. 277 (2011) 149–153.
[102] K.S. Liu, H.G. Fu, K.Y. Shi, F.S. Xiao, L.Q. Jing, B.F. Xin, J. Phys. Chem. B 109 (2005) 18719–18722.
[103] V. Iliev, D. Tomova, L. Bilyarska, G. Tyuliev, J. Mol. Catal. A: Chem. 263 (2007) 32–38.
[104] Y. Wang, J. Yu, W. Xiao, Q. Li, J. Mater. Chem. A 2 (2014) 3847–3855.
[105] (a) Q.J. Xiang, J. Yu, M. Jaroniec, Nanoscale 3 (2011) 3670–3678;
(b) X. Wang, L.J. Zhi, K. Mullen, Nano Lett. 8 (2008) 323–327.
[106] (a) A. Mitsionis, T. Vaimakis, C. Trapalis, N. Todorova, D. Bahnemann, R. Dillert, Appl. Catal. B: Environ. 106 (2011) 398–404;
(b) J. Yu, Y. Hai, B. Cheng, J. Phys. Chem. C 115 (2011) 4953–4958.
[107] V. Subramanian, E.E. Wolf, P.V. Kamat, J. Phys. Chem. B 107 (2003) 7479–7485.
[108] (a) K.S. Novoselov, A.K. Geim, S.V. Morozov, D. Jiang, Y. Zhang, S.V. Dubonos, I.V. Grigorieva, A.A. Firsov, Nature 438 (2005) 197–200;
(b) E. Vasilaki, I. Georgaki, D. Vernardou, M. Vamvakaki, N. Katsarakis, Appl. Surf. Sci. 353 (2015) 865–872.
[109] V. Iliev, D. Tomova, S. Rakovsky, Desalination 260 (2010) 101–106.
[110] G. Burgeth, H. Kisch, Coord. Chem. Rev. 230 (2002) 41–47.
[111] N. Pugazhenthiran, S. Murugesan, P. Sathishkumar, S. Anandan, Chem. Eng. J. 241 (2014) 401–409.
[112] (a) T. Kiyonaga, Q. Jin, H. Kobayashi, H. Tada, Chem. Phys. Chem. 10 (2009) 2935–2938;
(b) T. Akita, K. Tanaka, M. Kohyama, M. Haruta, Surf. Interface Anal. 40 (2008) 1760–1763;

(c) I.M. Arabatzis, T. Stergiopoulos, D. Andreeva, S. Kitova, S.G. Neophytides, P. Falaras, J. Catal. 220 (2003) 127–135.
[113] M. Daous, V. Iliev, L. Petrov, J. Mol. Catal. A: Chem. 392 (2014) 194–201.
[114] (a) S. Livraghi, M.C. Paganini, E. Giamello, A. Selloni, C. Di Valentin, G.F. Pacchioni, J. Am. Chem. Soc. 128 (2006) 15666–15671;
(b) S.S. Thind, G. Wu, A. Chen, Appl. Catal. B: Environ. 111–112 (2012) 38–45.
[115] (a) M. Diak, E. Grabowska, A. Zaleska, Appl. Surf. Sci. 347 (2015) 275–285;
(b) W. Dong, F. Pan, L. Xu, M. Zheng, C.H. Sow, K. Wu, G.Q. Xu, W. Chen, Appl. Surf. Sci. 349 (2015) 279–286;
(c) M.M. Gui, S.P. Chai, A.R. Mohamed, Appl. Surf. Sci. 319 (2014) 37–43;
(d) J. Fu, S. Cao, J. Yu, J. Materiomics 1 (2015) 124–133.
[116] H. Zhou, L. Ding, T. Fana, J. Ding, D. Zhang, Q. Guo, Appl. Catal. B: Environ. 147 (2014) 221–228.
[117] H. Tada, T. Mitsui, T. Kiyonaga, T. Akita, K. Tanaka, Nat. Mater. 5 (2006) 782–786.
[118] H. Zhu, B. Yang, J. Xu, Z. Fu, M. Wen, T. Guo, S. Fu, J. Zuo, S. Zhang, Appl. Catal. B: Environ. 90 (2009) 463–469.
[119] K. Kalyanasundaram, E. Borgarello, M. Gratzel, Helv. Chim. Acta 64 (1981) 362–366.
[120] F. Wang, Y. Jiang, A. Gautam, Y. Li, R. Amal, ACS Catal. 4 (2014) 1451–1457.
[121] (a) G. Liu, Y.N. Zhao, C.H. Sun, F. Li, G.Q. Lu, H.M. Cheng, Angew. Chem., Int. Ed. 47 (2008) 4516–4520;
(b) N. Feng, A. Zheng, Q. Wang, P. Ren, X. Gao, S.B. Liu, Z. Shen, T. Chen, F. Deng, J. Phys. Chem. C 115 (2011) 2709–2719.
[122] (a) N. Feng, Q. Wang, A. Zheng, Z. Zhang, J. Fan, S.B. Liu, J.P. Amoureux, F.J. Deng, J. Am. Chem. Soc. 135 (2013) 1607–1616;
(b) K.Y. Jung, S.B. Park, S.K. Ihm, Appl. Catal. B: Environ. 51 (2004) 239–245.
[123] (a) H.M.S. Suh, J.R. Choi, H.J. Hah, S.M. Koo, Y.C. Bae, J. Photochem. Photobiol. A: Chem. 163 (2004) 37–44;
(b) H. Zhang, C. Liang, J. Liu, Z. Tian, G. Wang, W. Cai, Langmuir 28 (2012) 3938–3944;
(c) X.F. Lei, X.X. Xue, H. Yang, Appl. Surf. Sci. 321 (2014) 396–403;
(d) K. Dai, D. Li, L. Lu, Q. Liu, C. Liang, J. Lv, G. Zhu, Appl. Surf. Sci. 314 (2014) 864–871;
(e) K. Laohhasurayotin, S. Pookboonmee, Appl. Surf. Sci. 282 (2013) 236–244.
[124] (a) J. Yu, J. Xiong, B. Cheng, S. Liu, Appl. Catal. B: Environ. 60 (2005) 211–221;
(b) H.E. Chao, Y.U. Yuan, H.U. Xingfanga, A. Larbot, J. Eur. Ceram. Soc. 23 (2003) 1457–1464.
[125] (a) C. He, Y. Yu, X. Hu, A. Larbot, Appl. Surf. Sci. 200 (2002) 239–247;
(b) M.M. Viana, N.D.S. Mohallem, D.R. Miquita, K. Balzuweit, E. Silva-Pinto, Appl. Surf. Sci. 265 (2013) 130–136;
(c) A. Ramchiary, S.K. Samdarshi, Appl. Surf. Sci. 305 (2014) 33–39.
[126] J.C. Yu, J.G. Yu, W.K. Ho, Z.T. Jiang, L.Z. Zhang, Chem. Mater. 14 (2002) 3808–3816.
[127] M. Miyauchi, A. Nakajima, K. Hashimoto, T. Watanabe, Adv. Mater. 12 (2000) 1923–1927.
[128] E.S. Bardos, E. Petervari, V. Zein, A. Horvath, J. Photochem. Photobiol. A: Chem. 184 (2006) 221–227.
[129] H. Liu, X. Dong, G. Li, X. Su, Z. Zhu, Appl. Surf. Sci. 271 (2013) 276–283.
[130] K. Qian, W.X. Huang, Catal. Today 164 (2011) 320–324.
[131] E.S. Bardos, H. Czili, A. Horvath, J. Photochem. Photobiol. A: Chem. 154 (2003) 195–201.
[132] (a) P.D. Cozzoli, E. Fanizza, R. Comparelli, M.L. Curri, A. Agostiano, J. Phys. Chem. B 108 (2004) 9623–9630;
(b) T. Kiyonaga, T. Mitsui, M. Torikashi, M. Takekawa, T. Soejima, H. Soejima, H. Tada, J. Phys. Chem. B 110 (2006) 10771–10778.
[133] P. Christopher, D.B. Ingram, S. Linic, J. Phys. Chem. C 114 (2010) 9173–9177.
[134] (a) X. Liu, Z. Liu, J. Lu, X. Wu, B. Xu, W. Chu, Appl. Surf. Sci. 288 (2014) 513–517;
(b) J. Lv, H. Gao, H. Wang, X. Lu, G. Xu, D. Wang, Z. Chen, X. Zhang, Z. Zheng, Y. Wu, Appl. Surf. Sci. 351 (2015) 225–231.
[135] (a) S.Q. Sun, B. Sun, W. Zhang, D. Wang, Bull. Mater. Sci. 31 (2008) 61–66;
(b) D. Kong, J.Z.Y. Tan, F. Yang, J. Zeng, X. Zhang, Appl. Surf. Sci. 277 (2013) 105–110.
[136] K.S. Chen, X.R. Feng, R. Hu, Y.B. Li, K. Xie, Y. Li, H.S. Gu, J. Alloys Compd. 554 (2013) 72–79.
[137] (a) S. Lal, S. Link, N.J. Halas, Nat. Photon. 1 (2007) 641–648;
(b) N.F. Jaafar, A.A. Jalil, S. Triwahyono, J. Efendi, R.R. Mukti, R. Jusoh, N.W.C. Jusoh, A.H. Karim, N.F.M. Salleh, V. Suendo, Appl. Surf. Sci. 338 (2015) 75–84.
[138] (a) C. Zhao, B. Feng, Y. Li, J. Tan, X. Lu, J. Weng, Appl. Surf. Sci. 280 (2013) 8–14;
(b) J.H. Lia, B.F. Yan, X.S. Shao, S.S. Wang, Q.Q. Zhang, H.Y. Tian, Q.Q. Zhang, Appl. Surf. Sci. 324 (2015) 82–89.
[139] I. Piwonski, K. Kadziola, A. Kisielewska, K. Soliwoda, M. Wolszczak, K. Lisowska, N. Wronska, A. Felczak, Appl. Surf. Sci. 257 (2011) 7076–7082.
[140] T.C. Pan, S.H. Wang, Y.S. Lai, J.M. Jehng, S.J. Huang, Appl. Surf. Sci. 296 (2014) 189–194.
[141] Y. Xie, Y. Jin, Y. Zhou, Y. Wang, Appl. Surf. Sci. 313 (2014) 549–557.
[142] Z. Yong Bao, X. Liu, J. Dai, Y. Wu, Y.H. Tsang, D.Y. Lei, Appl. Surf. Sci. 301 (2011) 351–357.
[143] H. Li, Q. Cui, B. Feng, J. Wang, X. Lu, J. Weng, Appl. Surf. Sci. 284 (2013) 179–183.
[144] C. Baker, A. Pradhan, L. Pakstis, D.J. Pochan, S.I. Shah, J. Nanosci. Nanotechnol. 5 (2005) 244–249.
[145] Y. Ao, J. Xu, Y. Gao, P. Wang, C. Wang, J. Hou, J. Qian, Catal. Commun. 53 (2014) 21–24.
[146] V. Subramanian, E. Wolf, P.V. Kamat, J. Phys. Chem. B 46 (2001) 11439–11446.
[147] T. Hirakawa, P.V. Kamat, J. Am. Chem. Soc. 127 (2005) 3928–3934.
[148] H.M. Sung-Suh, J.R. Choi, H.J. Hah, S.M. Koo, Y.C. Bae, J. Photochem. Photobiol. A: Chem. 163 (2004) 37–44.
[149] (a) L. Sun, J. Li, C.L. Wang, S.F. Li, Y.K. Lai, H.B. Chen, C.J. Lin, J. Hazard. Mater. 171 (2009) 1045–1050;
(b) Y.X. Zhao, B.F. Yang, J. Xu, Z.P. Fu, M. Wu, F. Li, Thin Solid Films 520 (2012) 3515–3522.
[150] M.L. de Souza, P. Corio, Appl. Catal. B: Environ. 136–137 (2013) 325–333.
[151] L. Ren, Y. Zeng, D. Jiang, Catal. Commun. 10 (2009) 645–649.
[152] S.P. Deshmukh, R.K. Dhokale, H.M. Yadav, S.N. Achary, S.D. Delekar, Appl. Surf. Sci. 273 (2013) 676–683.
[153] K.H. Leong, B.L. Gan, S. Ibrahim, P. Saravanan, Appl. Surf. Sci. 319 (2014) 128–135.
[154] (a) S.T. Kochuveedu, Y.H. Jang, D.H. Kim, Chem. Soc. Rev. 42 (2013) 8467–8493;
(b) X. Lang, X. Chen, J. Zhao, Chem. Soc. Rev. 43 (2014) 473–486.
[155] (a) J. Yu, Q. Xiang, M. Zhou, Appl. Catal. B: Environ. 90 (2009) 595–602;
(b) L. Qi, J. Yu, G. Liu, P.K. Wong, Catal. Today 224 (2014) 193–199.
[156] Y. Xu, H. You, Appl. Surf. Sci. 321 (2014) 481–487.
[157] D. Chen, Q. Chen, L. Ge, L. Yin, B. Fan, H. Wang, H. Lu, H. Xu, R. Zhang, G. Shao, Appl. Surf. Sci. 284 (2013) 921–929.
[158] J.A.G. Gallardo, J.L. Gervasoni, L. Kover, J. Nanosci. Nanotechnol. 12 (2012) 9271–9276.
[159] H. Guan, X. Wang, Y. Guo, C. Shao, X. Zhang, Y. Liu, R. Louh, Appl. Surf. Sci. 280 (2013) 720–725.
[160] K. Kadzioła, I. Piwonski, A. Kisielewska, D. Szczukocki, B. Krawczyk, J. Sielski, Appl. Surf. Sci. 288 (2014) 503–512.
[161] Y. Liu, C.Y. Liu, J.H. Wei, R. Xiong, C.X. Pan, J. Shi, Appl. Surf. Sci. 256 (2010) 6390–6394.
[162] T. Nonami, H. Hase, K. Funakoshi, Catal. Today 96 (2004) 113–118.
[163] S. Pei Lim, A. Pandikumar, N.M. Huang, H.N. Lim, G. Gu, T.L. Ma, RSC Adv. 4 (2014) 48236–48244.
[164] S. Pany, K.M. Parida, B. Naik, RSC Adv. 3 (2013) 4976–4984.
[165] J.M. Kroon, N.J. Bakker, H.J.P. Smit, P. Liska, K.R. Thampi, P. Wang, S.M. Zakeeruddin, M. Gratzel, A. Hinsch, S. Hore, U. Wurfel, R. Sastrawan, J.R. Durrant, E. Palomares, H. Pettersson, T. Gruszecki, J. Walter, K. Skupien, E. Tulloch, Prog. Photovolt. 15 (2007) 1–18.
[166] M. Ni, M.K.H. Leung, D.Y.C. Leung, K. Sumathy, Renew. Sustain. Energy Rev 11 (2007) 401–425.
[167] T. Wang, Z. Luo, C. Li, J. Gong, Chem. Soc. Rev. 43 (2014) 7469–7484.
[168] S. Zhang, F. Peng, H. Wang, H. Yu, S. Zhang, J. Yang, H. Zhao, Catal. Commun. 12 (2011) 689–693.
[169] D.B. Ingram, S. Linic, J. Am. Chem. Soc. 133 (2011) 5202–5205.
[170] (a) A.O. Govorov, J. Lee, N.A. Kotov, Phys. Rev. B 76 (2007) 125308;
(b) P. Anger, P. Bharadway, L. Novotny, Phys. Rev. Lett. 96 (2006) 113002.
[171] J.T. Yates Jr., Surf. Sci. 603 (2009) 1605–1612.
[172] Z. Zhang, J.T. Yates Jr., J. Phys. Chem. C 114 (2010) 3098–3101.
[173] T. Harifi, M. Montazer, Appl. Catal. A: Gen. 473 (2014) 104–115.
[174] (a) J. Zhu, F. Chen, J. Zhang, H. Chen, M. Anpo, J. Photochem. Photobiol. A: Chem. 180 (2006) 196–204;
(b) T. Sun, E. Liu, X. Liang, X. Hu, J. Fan, Appl. Surf. Sci. 347 (2015) 696–705.
[175] W. Wang, J. Zhang, F. Chen, D. He, M. Anpo, J. Colloid Interface Sci. 323 (2008) 182–186.
[176] X. Fan, J. Fan, X. Hu, E. Liu, L. Kang, C. Tang, Y. Ma, H. Wu, Y. Lia, Ceram. Int. 40 (2014) 15907–15917.
[177] Y.L. Min, K. Zhang, W. Zhoa, F.C. Zheng, Y.C. Xhen, Y.G. Zhang, Chem. Eng. J. 193–194 (2012) 203–210.
[178] B.Z. Tian, C.Z. Li, J.L. Zhang, Chem. Eng. J. 191 (2012) 402–409.
[179] T. Sun, E. Liu, J. Fan, X. Hu, F. Wu, W. Hou, Y. Yang, L. Kang, Chem. Eng. J. 228 (2013) 896–906.
[180] Y.Z. Yang, C.H. Chang, H. Idriss, Appl. Catal. B: Environ. 67 (2006) 217–222.
[181] M.A. Khan, S.I. Woo, O.B. Yang, Int. J. Hydrogen Energy 33 (2008) 5345–5351.
[182] H. Liu, L. Deng, C. Sun, J. Li, Z. Zhu, Appl. Surf. Sci. 326 (2015) 82–90.
[183] Q. Zhang, D.Q. Lima, I. Lee, F. Zaera, M.F. Chi, Y.D. Yin, Angew. Chem. Int. Ed. 50 (2011) 7088–7092.
[184] Q. Zhang, I. Lee, J.P. Ge, F. Zaera, Y.D. Yin, Adv. Funct. Mater. 20 (2010) 2201–2214.
[185] J.N. Ge, Q. Zhang, T.R. Zhang, Y.D. Yin, Angew. Chem. Int. Ed. 47 (2008) 8924–8928.
[186] C. Liu, D. Yang, Y. Jiao, Y. Tian, Y.G. Wang, Z.Y. Jiang, ACS Appl. Mater. Interfaces 5 (2013) 3824–3832.
[187] B. Xi, X. Chu, J. Hu, C.S. Bhatia, A.J. Danner, H. Yang, Appl. Surf. Sci. 311 (2014) 582–592.
[188] T.T.Y. Tan, C.K. Yip, R. Beydoun, R. Amal, Chem. Eng. J. 95 (2003) 179–186.
[189] (a) W.A. Jacoby, P.C. Maness, E.J. Wolfrum, D.M. Blake, J.A. Fennell, Environ. Sci. Technol. 32 (1998) 2650–2653;
(b) K. Sunada, Y. Kikuchi, K. Hashimoto, A. Fujishima, Environ. Sci. Technol. 32 (1998) 726–728.
[190] J. Yu, G. Dai, B. Huang, J. Phys. Chem. C 113 (2009) 16394–16401.
[191] Z.H. Shah, J. Wang, Y. Ge, C. Wang, W. Mao, S. Zhang, R. Lu, J. Mater. Chem. A 3 (2015) 3568–3575.
[192] K. Kawahara, K. Suzuki, Y. Ohko, T. Tatsuma, Phys. Chem. Chem. Phys. 7 (2005) 3851–3855.

[193] T.X. Wu, G.M. Liu, J.C. Zhao, H. Hidaka, N. Serpone, J. Phys. Chem. B 102 (1998) 5845–5851.
[194] J. Zhou, Y. Cheng, J. Yu, J. Photochem. Photobiol. A: Chem. 223 (2011) 82–87.
[195] P. Wang, B.B. Huang, X.Y. Qin, X.Y. Zhang, Y. Dai, J.Y. Wei, M.H. Whangbo, Angew. Chem. Int. Ed. 47 (2008) 7931–7933.
[196] H. Xu, H.M. Li, J. Xia, S. Yin, Z. Luo, L. Liu, L. Xu, ACS Appl. Mater. Interface 3 (2011) 22–29.
[197] M. Bowker, D. James, P. Stone, R. Bennett, N. Perkins, L. Millard, J. Greaves, A. Dickinson, J. Catal. 217 (2003) 427–433.
[198] A.T. Kuvarega, R.W.M. Krause, B.B. Mamba, J. Phys. Chem. C 115 (2011) 22110–22120.
[199] T. Butburee, Y. Bai, J. Pan, X. Zong, C. Sun, G. Liu, L. Wang, J. Mater. Chem. A 2 (2014) 12776–12784.
[200] S. Linic, P. Christopher, D.B. Ingram, Nat. Mater. 10 (2011) 911–921.
[201] M. Rycenga, M.R. Langille, M.L. Personick, T. Ozel, C.A. Mirkin, Nano Lett. 12 (2012) 6218–6222.
[202] N. Mirsaleh-Kohan, V. Iberi, P.D. Simmons Jr., N.W. Bigelow, A. Vaschillo, M.M. Rowland, M.D. Best, S.J. Pennycook, D.J. Masiello, B.S. Guiton, J.P. Camden, J. Phys. Chem. Lett. 3 (2012) 2303–2309.
[203] M. Haggui, M. Dridi, J. Plain, S. Marguet, H. Perez, G.C. Schatz, G.P. Wiederrecht, S.K. Gray, R. Bachelot, ACS Nano 6 (2012) 1299–1307.
[204] M. Rycenga, X. Xia, C.H. Moran, F. Zhou, D. Qin, Z.Y. Li, Y. Xia, Angew. Chem. 123 (2011) 5587–5591.
[205] J. Poanpranot, K. Kontapakdee, P. Praserthdam, J. Phys. Chem. B 110 (2006) 8019–8024.
[206] B. Lim, H. Kobayashi, T. Yu, J. Wang, M.J. Kim, Z.Y. Li, M. Rycenga, Y. Xia, J. Am. Chem. Soc. 132 (2010) 2506–2507.
[207] M.O. Nutt, K.N. Heck, P. Alvarez, M.S. Wong, Appl. Catal. B: Environ. 69 (2006) 115–125.
[208] J.G. Chen, C.A. Menning, M.B. Zellner, Surf. Sci. Rep. 63 (2008) 201–254.
[209] G.R. Bamwenda, S. Tsubota, T. Nakamura, M. Haruta, J. Photochem. Photobiol. A: Chem. 89 (1995) 177–189.
[210] A. Golabiewska, W. Lisowski, M. Jarek, G. Nowaczykc, A.Z. Jurek, A. Zaleska, Appl. Surf. Sci. 317 (2014) 1131–1142.
[211] Z. Zhang, C. Xue, A. Li, S.W. Cao, M. Bosman, S. Li, C. Xue, Nanoscale 6 (2014) 5217–5222.
[212] Z. Zhang, S.W. Cao, Y. Liao, C. Xue, Appl. Catal. B: Environ. 162 (2015) 204–209.
[213] A. Jureka, Z. Wei, I. Wysocka, P. Szweda, E. Kowalska, Appl. Surf. Sci. 353 (2015) 317–325.